institut de physique nucléaire
LABORATOIRE ASSOCIÉ A L'IN2P3

IPNO–DRE 85.14

EXPERIMENTAL SEARCH OF NON STRANGE NARROW ISOVECTOR DIBARYONS

B.TATISCHEFF, P. BERTHET, M.P. COMBES–COMETS, J.P. DIDELEZ, R. FRASCARIA, Y. LE BORNEC, A. BOUDARD, J.M. DURAND, M. GARCON, J.C. LUGOL, Y. TERRIEN, R. BEURTEY and L. FARVACQUE

UNIVERSITÉ PARIS-SUD
I.P.N. BP n° 1 - 91406 ORSAY

IPNO-DRE 85.14

EXPERIMENTAL SEARCH OF NON STRANGE NARROW ISOVECTOR DIBARYONS

B.TATISCHEFF, P. BERTHET, M.P. COMBES-COMETS, J.P. DIDELEZ, R. FRASCARIA, Y. LE BORNEC, A. BOUDARD, J.M. DURAND, M. GARCON, J.C. LUGOL, Y. TERRIEN, R. BEURTEY and L. FARVACQUE

EXPERIMENTAL SEARCH OF NON STRANGE NARROW ISOVECTOR DIBARYONS

B. TATISCHEFF, P. BERTHET, M.P. COMBES-COMETS, J.P. DIDELEZ, R. FRASCARIA, Y. LE BORNEC

Institut de Physique Nucléaire, F-91406 Orsay Cedex, France

A. BOUDARD, J.M. DURAND, M. GARCON, J.C. LUGOL, Y. TERRIEN

Departement de Physique Nucléaire à Moyenne Energie, Centre d'Etudes Nucléaires de Saclay, F-91191 Gif-sur-Yvette Cedex, France

R. BEURTEY and L. FARVACQUE

Laboratoire National Saturne, Centre d'Etudes Nucléaires de Saclay, F-91191 Gif-sur-Yvette Cedex, France.

Abstract : Missing mass spectra from $^3He(p,d)X$ at $T_p = .75$ GeV ($\theta_{lab} = 22°$, 32° and 40°) and $T_p = .925$ GeV ($\theta_{lab} = 30°$, 40°) have been measured. Missing mass spectra from $p(^3He, d)X$ at $T_{^3He} = 2.7$ Gev and $\theta_{lab} = 18°$ havealso been measured. The experiments have been carried out with a high missing mass resolution in order to detect possible narrow structures associated with B = 2, T = 1 quantum numbers Such structures have been found, with the following masses and widths .

$M_X = 2.240 \pm 0.005$ $(\Gamma_{1/2} \approx 0.016 \pm 0.003)$ GeV
$M_X = 2.192 \pm 0.003$ $(\Gamma_{1/2} \approx 0.025 \pm 0.006)$ GeV and
$M_X = 2.124 \pm 0.003$ $(\Gamma_{1/2} \approx 0.025 \pm 0.002)$ GeV.

There is also an indication for another narrow structure at $M_X \approx 2.155$ GeV. A broad structure with mass close to $M_X \approx 2.17$ GeV, the mass of free N+Δ, and a width close to $\Gamma_{1/2} \approx 0.1$ GeV is observed. The masses of the narrow structures are shown to agree with a rotational like mass formula $M = M_0 + M_1 J(J+1)$, J being the associated spin. The observed peaks might be related to six quark states.

NUCLEAR REACTIONS $^3He(p,d)X$ $T_p = .925$, .750 GeV, $p(^3He, d)X$ $T_{^3He} = 2.7$ GeV. Missing mass spectra measured. Deduced isovector dibaryons.

1. INTRODUCTION

The spectroscopy of dibaryonic resonances has been strongly stimulated over the last ten years, by theoretical as well as experimental studies. It was shown that six quarks confined in a bag, produce as a consequence many exotic states [1] neither predicted before nor experimentally observed. At the same time, nucleon-nucleon experiments from Argonne (ZGS) and deuteron photodisintegration from Tokyo revealed unexpected features which were related to dibaryonic resonances.

The NN studies started at Argonne (ZGS) [2] showed structures in $\Delta\sigma_L$, $\Delta\sigma_T$, C_{LL} scattering in p-p mainly but also in some indirect p-n (through p-d) measurements. The new experiments from LAMPF [3], SIN [4], Saclay [5], Leningrad [6] and TRIUMF [7] confirm the observed structures for energies lower than $T_p = 0.8$ GeV. These were interpreted as being the signature of $^1D_2$ and $^3F_3$ dibaryonic resonances from the various phase shift analyses [8]. The inelastic scattering [9] was particularly interesting since it was shown that calculations based on unitary relativistic three body models [11] are unable to reproduce the experimental data, especially in the case of $\Delta\sigma_L^{inel.}$ ($pp \rightarrow NN\pi$), but also for spin transfer parameters K_{NN} and K_{LL} [10] and others [24].

Several theoretical predictions [11] have been made which generally conclude that the structures in the data and loops in the Argand plots were produced by non-resonant dynamics coupling to NΔ and NNπ. Although generally believed, this negative conclusion on the existence of the dibaryon resonances was not supported by all calculations [12]. A recent work from Jauch et al. [13] in particular showed that an admixture of dibaryon resonance L = 1, $J^P = 3^-$, in addition to calculations from the Deck model leads to a good description of such data as $\Delta\sigma_L^{inel.}$ and inelastic total NN cross sections otherwise badly described.

The pion-deuteron physics concerns mainly the $pp \rightarrow d\pi^+$ studies and elastic π-d scattering with measurements of differential cross sections, vector polarisation iT_{11} and tensor polarisation T_{20}. The $pp \rightarrow d\pi^+$ experiments, which study analyzing powers and differential cross sections have been developed [14] at Saturne (Saclay), LAMPF, SIN, TRIUMF and Gatchina. A detailed discussion can be found in Seth [29]. These results have been analyzed [15] using eith

phase shifts or coupled channel equations allowing a simultaneous analysis of NN, πd, NΔ and NNπ channels. Although the fit between measured and calculated data is poor, it is not possible to reach a conclusion on the existence of dibaryons from these discrepancies. The vector analyzing power iT_{11} in the πd → pp reaction has been measured at SIN [23]. The qualitative agreement found with theoretical predictions does not require us to invoke the existence of dibaryons. Similarly the lack of agreement between the measurements [24] of the spin correlation parameter A_{NN} in pp → dπ⁺ and theoretical predictions prevents us from drawing any conclusion about dibaryons.

The iT_{11} parameter measurements in elastic π–d scattering have been carried out at SIN, using polarized deuterium targets. While the first data [18] showed the oscillatory behaviour often attributed to dibaryons, more recent data [19] are smooth. The analysis has been done within relativistic three body theory and Faddeev amplitudes [20].

The tensor polarization T_{20} in elastic π–d scattering has been measured at SIN [21] and LAMPF [22]. The experimental results are still contradictory, although very close incident energies and angles were investigated. The data show oscillations at some energies at SIN but a smooth and negative behaviour at LAMPF.

The polarization of the proton produced in deuteron photodisintegration measurements in Tokyo [25] was, together with NN studies, the earliest contribution to the dibaryon hunt. At least two resonances, one isoscalar and one isovector have been found. The first Japanese results appear however to be in contradiction [27] either with theoretical calculations or new photodisintegration measurements. After analysis of new differential cross sections measurements of γd → pn, γd → π°d and γd → pX reactions, the authors were not able to draw a clear conclusion about the existence of dibaryon resonances.

The above discussion deals with broad dibaryons with widths of the order of $\Gamma_{1/2} \approx 100$–200 MeV. But interest has however moved gradually toward narrow resonances. McGregor [30], analyzing the masses and quantum numbers of the resonances of the structures from NN experiments, concluded they were rotational levels based on a virtual ppπ dibaryon bound state at 2.02 GeV. He predicted a $^3P_1$ level at 2.06 GeV. Wainer and Lomon [31], analyzing the constraints imposed by all the experimental informations in the energy region through the phase shifts, found that the required width of such a postulated

resonance should be $\Gamma < 0.3$ MeV. Later Mulders [32], using the P matrix formalism to connect the short range part of the interaction described by six quarks in a bag with the long range part of the interaction (the long range part of the Paris potential) predicted some very narrow dibaryonic states.

Experimental studies were undertaken which led to negative results. Total n-p cross sections have been measured at LAMPF [33]studying invariant masses lying between $1.93 < \sqrt{s} < 2.23$ GeV. Although the statistics and energy resolution were good, no evidence for narrow resonance was reported. Other negative studies have been reported which will be discussed more carefully later. They are the p-p elastic scattering cross-section at $\theta_{CM} = 90°$ [34], using an internal gas jet target at Saturne (Saclay) $2.12 < \sqrt{s} < 2.40$ GeV, the $d(\pi^+, p)p$ relative yield [35] measured at LAMPF at $\theta_{CM} = 90° \pm 2°$, in the range $2.07 < \sqrt{s} < 2.28$ GeV and the measurement of analyzing power in $d(p, p')pn$ reaction from LAMPF [35] at $\theta_{lab} = 18°$, in the range $2.00 < \sqrt{s} < 2.07$ GeV.

Measurements with positive signals are from four kinds of experiments :

a) Preliminary reports from our experiments [36], where missing mass spectra have been measured using transfer reactions.

b) Deuteron [37] and ^{4}He [38] break-up experiments performed at Dubna have revealed narrow structures at different invariant masses.

c) Some results from deuterium photodisintegration measurements performed at ALS (Saclay) [26] and at Bonn [43].

d) An inclusive $^{12}C(\pi^-, 2p)X$ reaction [44] performed at Dubna.

Various review articles have been published on this subject of dibaryonic resonances [29].

2. EXPERIMENTAL METHOD

The experiment was performed at the Laboratoire National Saturne (LNS) using the proton beam delivered by the Saturne synchrotron. Some preliminary data were taken in november 1979. More extensive measurements were done one year later in november 1980. In both studies, differential cross sections for ^{3}He(p,d)X were measured. Then, in june 1983, complementary measurements were done by exchanging the incident and target particles : p(^{3}He,d)X at roughly the same center of mass energy. In all three cases, the outgoing deuteron was detected in the spectrometer SPES1 and identified by a 5.6 m basis time of flight added to the p/z measurement. The missing mass M_X was given by the angle and momentum of the deuteron. One magnetic field setting covered $\approx$3% of $\Delta p/p$ ($\approx$30 MeV in M_X). Many different settings with large overlaps were used in order to get a large missing mass spectrum of several hundreds MeV. The different parts of the experiment description will be detailed in the following paragraphs.

2.1. BEAM TRANSPORT AND SPECTROMETER

Figure 1) shows the beam line corresponding to the energy loss SPES1 spectrometer [47]. Three quadrupoles located before the target allow the adjustement of the beam line for the kinematics of the studied reaction. In our case, due to the relatively small dimensions of the cryogenic target, we have focussed the beam onto the target. It follows that the currents in all quadrupoles remain constant for a given energy. The sextupoles were not used, and the collimators were not moved during the measurements at a given angle. The current in the spectrometer SPES1 was adjusted to get the measurements for different momenta of the detected particles which correspond to different missing masses for the undetected B = 2 system (X). The magnetic field in the spectrometer and analyzer was regulated within some parts in 10^5, and checked using NMR signals.

The quadrupole located between the target and the spectrometer, was adjusted in order to keep the vertical angular aperture $\Delta\theta_v$ constant.

The position of the beam was determined using wire chambers and secondary emission detectors. The centering on the target was also checked by measuring the counting rate as a function of the horizontal position of the beam. The stability in position during the measurements was controled with a localisation wire chamber located before the target, and checked between every data taking. The stability was better than ± 1 mm.

2.2. TARGET

The liquid ^3He target was constructed by the IPN cryogenic service [45]. The target cell was a cylinder 50 mm in diameter and 68.8 mm in length kept at a pressure of 300 torr. The corresponding temperature was 2°425 ± 0°025, and the thickness $\rho d = 509 \pm 9$ mg/cm^2. Three windows were crossed successively by the protons and deuterons at small angles : stainless steel (20 μm), aluminium (10 μm) and kapton (75 μm). The L H_2 target was constructed by the LNS cryogenic group. Its thickness was 205 ± 20 mg/cm^2.

2.3. MONITORING

Two different telescopes and a secondary electron emission chamber were mainly used for the beam calibration. The telescope M1, located in the vertical plane at 30° from the beam direction, was made of six scintillation counters. The telescope M3 was made of four scintillation counters heavily shielded by lead, and located in the horizontal plane at 90° from the beam. A secondary emission monitor was located before the target in the direct beam, and not viewed by the spectrometer for the angles considered here.

The ratios of the counting rates between these three monitors was checked to be stable within ± 1 %. In the few cases where this limit was exceeded they have been corrected and 20 % of that correction introduced in the error bar. The absolute calibration was done at each energy by means of the activation reaction $C(p,X)^{11}C$ or $C(^3He, X)^{11}C$ [48]. A typical value of the beam intensity was 15 nA at large angle decreasing to 0.25 nA at small angle. The beam duration for 0.925 GeV protons was close to 600 ms every 1320 ms.

2.4. DETECTORS

Four double drift chambers [49] were used to determine the trajectory of each detected deuteron (see fig. 2). Each chamber consists of one drift cell of 50 cm long corresponding to $\Delta P/P = \pm 2$ %. In fact due to the loss of precision at both ends of the detection, only a part of the detection covering roughly 3 % of the mean momentum was used. The trigger consisted of 5 planes of scintillation counter hodoscopes. The time-of-flight information for particle identification was measured between planes F and A on a 5.6 meters basis. Figure 3 shows two typical time of flight spectra, corresponding to the situations without protons on detection, and with a large amount of protons. Note the enhancement of the scale in order to point out the base-line of the spectra.

2.5. DATA ACQUISITION

Since the best kinematical conditions to look for possible narrow structures are not known, measurements have been done at different angles and energies. Conditions corresponding to large momentum transfers seem to be favorable because they correspond to a frontal scattering. However the production cross section may be larger at smaller angles. It is obviously the ratio of the production cross section versus the cross section of the background which is the important factor.

Data for the reaction $^3He(p,d)X$ have been measured at two energies T_p = .925 and T_p = .750 GeV and different angles, from $M_x \approx 1.88$ to $M_x \approx 2.35$ GeV. At T_p = .925 GeV, the lab. deuteron angles were 40° and 30°, and at T_p = .750 GeV, θ_d = 40°, 32° and 22°.

Measurements were also done at 6° for T_p = .75 GeV showing in particular a peak at $M_x \approx 1.9$ GeV corresponding to a quasi-free scattering of the incident proton on a deuteron substructure of ^3He. The data show also a peak for M_x = 2.09 GeV corresponding to the quasi-free $pp \rightarrow d\pi^+$ reaction. For this range of missing masses the magnetic field in the spectrometer is larger than that corresponding to elastically scattered protons, which occurs at M_x = 2.15 GeV. The proton flux was then so large for this small angle, that measurements were stopped for M_x = 2.13 GeV. At this small angle furthermore, the spectrometer coils were protected from direct beam by an uranium block which produced a large background in the detection.

Consequently the data for T_p = .750 GeV and θ_d = 6°, will not be presented later.

Measurements were also done at θ_d = 14° for T_p = .925 GeV and T_p = .750 GeV. At this angle the data were more sparse at .925 GeV. Moreover this angle corresponds to the maximum laboratory angle possible for the quasi-free pp → $d\pi^+$ reaction. The deuterons so produced contaminated the spectrum in a large range of missing masses, starting at $M_X \approx 2.2$ GeV. This contamination appeared unfortunately to be not negligible, especially at T_p = .750 GeV, in comparison with the small yield of the expected structures, so the data for this angle and the two energies will not be discussed later.

For the p(^{3}He, d)X reaction data have been measured at $T_{^3He}$ = 2.7 GeV and θ_d = 18° lab. This energy corresponds to total CM energy close to the previous one. The lower branch of the kinematical curve has been chosen so that the θ_{CM} for (p, d) system have neighbouring values for both reactions.

2.6. DATA REDUCTION

2.6.1. *Proton contamination*

At all angles, the proton flux increases very quickly for the magnetic fields corresponding to elastic scattering on ^{3}He. The protons were cut electronically by the time of flight, but since their flux was larger than deuteron flux by a factor up to 50, we have checked that no peak in the deuteron spectrum occurs due to a very small leak of the protons in the deuteron time of flight peak. Since a proton peak could only occur for elastic scattering, we have shown the corresponding missing mass in the figures by an arrow noted p. We can see that no peak appears for these particular conditions. In figure 3 two typical time of flight spectra are shown, demonstrating that the proton contamination under the deuteron peak is equal or less than 2 % depending on the magnetic field value in the spectrometer.

2.6.2. *Angular acceptance*

Slits at the entrance of the spectrometer defined the following angular apertures : $\Delta\theta_V$ = 51.8 mrad, $\Delta\theta_H$ = 48.9 mrad. However due to the size of the detection, some trajectories were not detected. Each trajectory was defined by the eight chambers, determining its angle : θ_f, and its intersection y with a virtual

plane. Then the analyzing code using θ_f and y calculated the corresponding missing mass M_x and the angle of the emitted deuteron from the target θ_d. All events for each run were plotted in a bi-dimensional spectrum $N = f(\theta_d, M_x)$. For a heavy target, without recoil, the focal plane is located in the middle of the drift chambers (Fig. 2) and the shape of the bi-dimensional spectrum defining the horizontal acceptance, looks very close to a parallelogram. For the reaction we have studied, the recoil is very important, especially at large angle. As the angle varied, the focal plane moved to infinity and came back from the forward direction. The trajectories undergo strong cuts at large angles for small missing masses and at small angle for large missing masses – as shown in figure 4. The computer code consequently calculated the horizontal opening angle –permitted by the detection– for each bin (corresponding to 1 MeV precision in energy scale of M_x) of each run. Both extremities of this parallelogram, which have small statistics and badly determining $\Delta\theta_H$, were omitted by software cuts. For each bin an error bar for the horizontal opening angle was computed (see later) simultaneously with the angle itself.

2.6.3. Summation of runs

In order to avoid possible systematic errors each spectrum results from several different runs with large overlap, as seen in figure 5. The data from adjacent spectrometer settings agree within the statistical uncertainties in the region of overlap. A spectrum is then obtained by mixing the different data using the usual statistical relations. The same analysis was done for full and empty targets (data corresponding to different windows), and subtracted. When not specified, the results correspond to full minus empty target measurements. At small angles the counts from the empty target were negligible in comparison with the full target, and consequently were measured less systematically. The subtraction was therefore not made. For the data shown later this is the case only for T_p = .750 GeV, θ_d = 22°.

2.6.4. Angular correction

Because of the shape of the acceptance (Fig. 4), all missing masses within a given run are measured with slightly different average scattering angles. However due to the large overlap of the runs, the final spectrum is insensitive to the angular correction (see fig. 5). A small correction was nevertheless applied to all data.

2.6.5. Losses due to counting rate

Dead time can produce a loss of counting rate at different stages of the data acquisition. This loss was measured on-line by the comparison of the number of events simulated on the detectors by a pulse generator and the number of events registered by the computer. The generator was triggered by a signal of a photomultiplier of a monitor telescope detector and therefore followed all beam intensity fluctuations. This correction was checked by repeating a measurement with a beam whose intensity was increased by a factor of 7. The final results after counting-loss corrections agree within a few percent. The proton intensity was varied for different production angles and usually adjusted to keep the dead time below 15 %.

2.6.6. *Error estimation*

The statistical errors are computed using different factors coming from full and empty target countings. The uncertainty on the horizontal aperture was taken to be $(NC + 0.5)^{-\frac{1}{2}}$ where NC corresponds to the number of channels in the angular axis of the bidimensionnal spectrum used to define the aperture itself. Sometimes a correction had to be introduced because the time of flight spectrum showed a non-negligible background under the deuteron time of flight peak. This correction was < 2 % and a term corresponding to 20 % of this correction factor was introduced in the error bar. In the same way 20 % of a possible factor correcting monitors fluctuation was also introduced. All these factors computed statistically gave the error bars plotted on the figures, typically less than or equal to ± 3 %, allowing us to conclude that a high statistics experiment had been undertaken. There is in addition, not introduced in the data shown, a systematic error coming principally from the absolute calibration of the monitors, but also from the vertical opening angle and the target thickness known to ± 1.8 %. It can be estimated to be ± 15 %.

2.6.7. *Missing mass resolution*

From kinematics we get the following relations :

$$\Delta M_X = \frac{\partial M_X}{\partial p_3} \Delta p_3 + \frac{\partial M_X}{\partial \theta_3} \Delta \theta_3$$

$$\text{with } \frac{\partial M_x}{\partial p_3} = \frac{p_1 \cos\theta_3 - E_0\beta_3}{M_x} \text{ and } \frac{\partial M_x}{\partial \theta_3} = -\frac{p_1 p_3 \sin\theta_3}{M_x}$$

where $E_0 = E_1 + m_2$ and the notations 1,2,3,x refer to the projectile, target, detected deuteron and missing mass, respectively. The contribution of $\partial M_x / \partial E_1$ is small and can be neglected.

The main contribution to ΔM_x comes from $(\partial M_x / \partial \theta_3)\Delta\theta_3$ because of the beam focusing conditions. This term increases with angle. For a given angle it decreases for increasing missing masses because M_x increases and simultaneously $p_3 \approx p_d$ decreases.

At two angles and energies (T_p = .925 MeV, $\theta_d = 40°$ and T_p = .750 GeV, $\theta_d = 32°$), the counting rate corresponding to protons elastically scattered on ^{3}He was small enough to allow its measurement (there were no cut applied by the electronics). The corresponding cross sections are plotted on figure 6 and compared with data from Legrand [65]. The $d\sigma/dt$ values agree with the interpolated values within 6 to 8 %. The energy resolution of these elastic proton peaks is used to check the computed values of the energy resolution which is strongly dependent on $\Delta\theta_3$. The resolutions agree roughly, which allows us to conclude that our energy resolution for the ^{3}He(p, d)X reaction varied from $\Delta M_x \approx 3$ MeV at $\theta_d = 22°$, to $\Delta M_x \approx 7$ to 8 MeV at $\theta_d = 40°$. These values are for large missing masses, close to $M_x \approx 2.24$ GeV, but are not very different for little smaller missing masses where structures have also been found. The missing mass resolution for p(^{3}He, d)X reaction at $\theta_d = 18°$ is close to 4 MeV. These values justify our choice of analyzing the data with a value of 1 MeV for each energy bin. Then, after having checked that no structure narrower than 10 MeV was present, an integration of the spectra was done, in order to increase the statistical precision. The data presented have been binned into 5 MeV intervals.

2.6.8. *Missing mass calibration*

There is a direct and known correspondence between the magnetic field measured by mean of NMR and the momentum of the detected deuterons. For a given spectrum an overall small correction constant has been applied to all data to correct for energy loss of protons and deuterons in the target. It usually ranges between minus 2 to minus 3 MeV. A very nice agreement with the ^{3}He mass had been found in the ^{3}He(p, p)^{3}He elastic scattering reported before. We conclude that our energies are correct to better than 2 MeV.

2.6.9. *Check of the computer code*

As previously mentioned the magnetic tapes were analysed on a UNIVAC 1110 computer. A large part of the T_p = .925 GeV, θ_d = 40° spectrum was reanalysed on the S.A.R. computer [51] (the LNS computer) with a different code and independent cuts, and the good agreement found between these two analysis can be seen in figure 7.

3. RESULTS

We present here the results from all our measurements. Whenever a narrow structure is observed, the following procedure has been followed to get the values quoted in table 1. First a polynomial fit has been carried out after having removed the five data points corresponding to structures. Then the number of standard deviations (S.D.) from the background has been computed using the relation

$$S.D. = \sum_i \left(N_{Ti} - N_{Bi}\right) / \Delta\sigma_i^2 \Big/ \left\{ \sum_i 1/\Delta\sigma_i^2 \right\}^{1/2}$$

where N_{Ti} corresponds to the total cross section for the data i, N_{Bi} the corresponding value for the background got by means of the polynomial fit described previously, and $\Delta\sigma_i^2 = \Delta\sigma_{Ti}^2 + \Delta\sigma_{Bi}^2 \approx 2\ \Delta\sigma_{Ti}^2$. $\Delta\sigma_{Ti}$ corresponds to the total error bar.

From the values of the standard deviations we deduced the confidence level (C.L.) of the peak. Values of masses, widths, cross sections and corresponding precisions are determined by the introduction into data of cross sections measured in the structure regions and making gaussian fits in addition to the previous polynomial fit. The method is not completely rigourous since the data are not quite independent. However their large number (see fig. 5) justify our analysis.

3.1. T_p = .925 GeV, θ_d = 40°

Two sets of data (N79 and N80) have been taken a year apart. A bump located close to M_X = 2.243 GeV is observed in the missing mass spectrum. The analysis of both sets of data, shown in figure 8. indicates a very good agreement. Indeed both have been quantitatively corrected for the background giving close values for M_X, $\Gamma_{1/2}$, and $d\sigma/dt$ as indicated on table 1.

The spectrum in figure 9 shows a broad bump corresponding to the quasi free pd → dp scattering of incident protons on a deuteron substructure of ^{3}He. It shows also an increase in background corresponding to the opening of the NΔ channel. The phase space has been calculated for X = pp and NΔ, but the first one gives a small contribution since it has to be normalised at low invariant masses $M_X \approx$ 2.0 GeV where the cross section is very small. The contribution of phase space X = NΔ ($\Gamma_{1/2}$ = .115 GeV), normalised to our data, is shown by dashed curve. It appears clearly to be unable to fit the measured cross sections.

Two narrow structures are clearly seen at M_X = 2.121 and 2.243 GeV.

3.2. T_p = .750 GeV, θ_d = 40°

For this lower energy, we see again a large bump corresponding to pd → dp, a small peak at 2.124 GeV, and another one at 2.192 GeV. The measurements have been stopped at a too small missing mass preventing a study of the structure seen previously at 2.240 GeV. The dashed curve corresponds again to the normalized phase space for X = NΔ ($\Gamma_{1/2} \approx$ .115 GeV) (Fig. 10), where it can be seen that there is no structure in this phase space spectrum at the corresponding masses. The empty target spectrum is shown in figure 11. There is no structure-no hole-in this spectrum at M_X = 2.124 and 2.192 GeV. The ratio of full to empty target countings for the two mentioned structures is larger than 5.1 and 4.5 respectively.

3.3. T_p = .925 GeV, θ_d = 30°

Apart from the pd → dp bump, some slightly excited structures are seen. Above 2.265 GeV, the lack of statistics prevents from any precise interpretation of the data (Fig. 12).

The arrows drawn at 2.192 and 2.240 GeV show that the spectrum is compatible with structures for these masses. It is not excluded also that a small but broad structure centered around 2.183 GeV ($\Gamma_{1/2} \approx 40$ MeV) lies below the weakly excited structures. Otherwise the subtraction of the two narrow structures, from background will leave a place for another one at $M_X \approx 2.16$ GeV with $\Gamma_{1/2} \approx 18$ MeV.

The phase space curve shown corresponds to NΔ final state ($\Gamma_{1/2} = .115$ GeV). A phase space prediction with four particles in the final state (d, p, p, and π) has also been calculated using the code FOWL [52]. Its predictions, normalized on the data, are similar to the one drawn on figure 12.

3.4. $T_p = .750$ GeV, $\theta_d = 32°$

The bump corresponding to pd → dp is the only dominant feature of this spectrum (Fig. 13). Within the error bars, there is no room here for any narrow or broad structure. The phase space for X = N + Δ, again does not fit the measured differential cross sections.

3.5. $T_p = .750$ GeV, $\theta_d = 22°$

The spectrum (Fig 14) shows the pd → dp bump, and a broad structure centered around M ≈ 2.14 GeV ($\Gamma_{1/2} \approx .115$ GeV) with $d\sigma/d\Omega \approx 142$ μb/sr. The full lines have at this stage been drawn by hand to guide the eye. The empty target cross-sections, which are very small for small angles, require only a few measurements. Both sets of data are presented on figure 14. No fit has been done on the data but arrows indicate the possibility of structures at 2.120, 2.155 and 2.240 GeV.

3.6. p(^{3}He,d)X reaction at $T_{^3He} = 2.7$ GeV

In order to check that the structures observed were not a consequence of possible parasitic scattering on some windows, or slits, a measurement of the reaction inverting the roles of beam and target seemed very useful. The energy was chosen in order to have a total center of mass energy as close to that of the previous reactions at $T_p = .925$ GeV as was allowed by the dipole of the transport

beam line. The laboratory angle for the detected deuterons $\theta_d = 18°$, corresponds to the only angular region free of $p(p,d)\pi^+$ reaction and, for the missing masses studied, far from the maximum of the laboratory angle (Fig. 15). The $p(p,d)\pi^+$ reaction quoted will be a quasi free reaction with a proton from incident ^3He particles having one third of the energy and momentum.

The results are plotted on figure 16. They show broad bumps centered around 2.17 GeV ($M_N + M_\Delta$), depending on the curve drawn to reproduce the background (Fig. 17), and a small structure centered around $M_X \approx 2.240$ GeV. Figure 18 shows phase space calculations for X = NN and NΔ normalized to our data. The NN final state phase space increases with M_X, in contradistinction to the $^3He(p,d)X$ reaction, since in $p(^3He,d)X$ the center-of-mass is moving quickly in the laboratory due to the large ratio of incident particle mass to the target particle. The full lines correspond to the background used to extract the cross sections of the narrow and broad structures.

In figure 15, three curves are drawn to show the kinematical conditions corresponding to $p(p,d)\pi^+$: the one without Fermi motion of a p in ^3He, and two others, with a p having a Fermi motion of ± 100 MeV/c along the beam direction. If we allow the Fermi motion of the projectile nucleon to have any direction, there is indeed a small probability that deuterons coming from this elementary process will enter the spectrometer. However their momentum distribution is wide and cannot give rise to a narrow structure as the one observed here. The same argument holds for the previous cases when the ^3He is the target nucleus : a contamination from the quasi free $pN \rightarrow d\pi$ reaction is possible at the lowest angle ($\theta_d = 22°$), but this cannot create narrow structures in the missing mass spectrum.

Now let us ask the question if the observed peak was produced by a parasitic target heavier than liquid hydrogen. Of course the data from the empty target have been subtracted. Moreover if the target is somewhat heavier than hydrogen, the momentum of the deuterons created by mean of $(^3He,d)$ reaction at $\theta_{lab} = 18°$ and $T_{^3He} = 2.7$ GeV, increases immediatly with the target mass to a value outside the experimental range. For example for $d(^3He,d)^3He$ g.s. $p_d = 3.65$ GeV, and in order to have $p_d = 1.35$ GeV, we have to consider an excited state in ^3He as high as 1.0 GeV ! We have therefore no explanation for the small shift of the missing mass with angle in the $p(^3He,d)X$ reaction, which can be purely accidental.

4. DISCUSSION

4.1. THE PEAK AT M_X = 2.24 GeV

It has been quantitatively determined from $p(^3He,d)X$ data at 17°64 and 18°, and with a small confidence level at 18°36. Both sets of data for $^3He(p,d)X$ reaction at T_p = .925 GeV and θ_d = 40° show a structure for this invariant mass with large confidence level (> 99 %). The masses deduced are stable if the data at 18°36 where small C. L. has been found, is omitted. The final mass value is M_X = 2.240 ± 0.005 GeV, with $\Gamma_{1/2}$ (FWHM) ≈ 18 ± 3 MeV.

No structure was seen for this invariant mass in the deuteron break-up experiment [37], but this mass corresponds to the limit of that experiment, where the counting rate for each bin is very small (< 10). Some other measurements done with high energy resolution, such as $d(p,p)pn$ [35], $d(\pi,p)p$ [35] or $d(\pi,n)d$ [21] have not been extended to an invariant mass as large as 2.24 GeV.

A structure at a mass $M_X \approx 2.230$ GeV having a width $\Gamma_{1/2} \approx 0.030$ GeV has been reported [26] previously from ALS, Saclay. It has been observed in the deuteron photodisintegration experiments $D(\gamma,p\pi^-)$. Jauch et al. [13], analyzing different NN data, have shown that an introduction of a dibaryon admixture I = 1, $J^P = 3^-$ to the Deck model helps to get a good agreement with experimental data for $\Delta\sigma_L(pp \to NN\pi)$ and various total cross sections $\sigma(NN \to NN\pi)$. They predicted a dibaryon mass of 2.236 GeV, precisely the one measured here, but with Γ_{tot} = 120 MeV and Γ_{el} = 26 MeV.

4.2. THE PEAK AT M_X = 2.124 GeV

Its mass, width and production cross section $d\sigma/dt$ for the $^3He(p,d)X$ reaction, has been determined at θ_d = 40° for both energies studied, and shown in figure 18 and table 1. There is also an indication for that mass at θ = 22°, T_p = .75 GeV.

In deuteron break up experiments [37], the structures observed at 2.137 ± 0.01 GeV (Mnp), 2.11 ± 0.02 GeV (Mnn) have masses consistant with 2.124 GeV. So is the structure observed at 2.137 ± 0.015 GeV (Mpp) in the ^4He break-up experiment (dppn final states), and at 2.126 ± 0.015 GeV (Mpp) ($pppp\pi^-n$ final state [38]).

No peak for such invariant mass was observed in d(π,'p) p [35] experiment. However we have to notice that the large t value t ≈ 0.4 GeV² seems not favourable for the excitation of this peak. It is close to the t value for p(³He, d)X reaction at $T_{^3He}$ = 2.7 GeV, θ_d = 18° (t = .32 GeV²) where that structure was also absent.

4.3. THE PEAK AT M_X = 2.192 GeV

It has been analyzed quantitatively at T_p = .750 GeV, θ_d = 40° (see Table 1), and pointed out in the spectrum shown at T_p = .925 GeV, θ_d = 30°. The t values for both cases are rather large (respectively - .627 GeV² and - .422 GeV²) and the extracted invariant cross section dσ/dt for .925 GeV, 30°, close to the value at .75 GeV, 40°. A peak at this mass value has never been seen previously.

4.4. THE PEAK AT M_X = 2.155 GeV

A peak at this mass value was not extracted quantitatively but pointed out in the spectrum T_p = .75 GeV, θ_d = 22°, with a full width at half maximum $\Gamma_{1/2} \approx 18$ MeV. A peak at this mass value has never been seen previously, but it is clear that its confidence level is not large.

4.5. THE BUMP AT $M_X \approx 2.17$ GeV

A large bump with a mass close to 2.17 GeV and a width of the order of $\Gamma_{1/2} \approx 110$ MeV was observed at T_p = .75 GeV, θ_d = 22° in the ³He(p, d)X reaction and $T_{^3He}$ = 2.7 GeV, θ_d = 18° in the p(³He, d)X reaction. In both cases the invariant cross sections dσ/dt are of the order of several hundred μb/GeV², typically two orders of magnitude larger than the narrow structures discussed before. These two reactions for the given angles and energies, have the smallest momentum transfers of the different experimental conditions of the data reported here (Fig. 20).

Since the broad bump was not observed for other angles and energies, we conclude that its excitation cross section is a quickly decreasing function of momentum transfer. Since its mass is close to the mass of free $M_N + M_\Delta$, and width close to the width of free Δ, we identify that broad bump with a classical N + Δ state bound by the strong interactions.

4.6. INELASTICITY OF THE NARROW STRUCTURES

Some NN experiments have been done with high statistical accuracy and energy resolution. Among them :

a) p-p differential cross section at 90°CM, with internal gas jet target from Saturne [34], where invariant masses from 2.12 to 2.40 GeV have been studied with high momentum transfer ($-.9 < -t < -.5$ GeV^2).

b) p-p analyzing powers using the radiography experimental set-up at LNS [54], where invariant masses from 2.18 to 2.33 GeV have been explored ($0.65 < T_p < 1.0$ GeV ; $16° < \theta^{lab} < 36°$).

c) σ_T(n-p) from LAMPF [33] though with less precise experimental conditions for invariant masses close to 2.2 GeV,

Since no narrow structure appeared in these high energy resolution experiments, we deduce that the corresponding elasticities are small.

4.7. RESULTS OBSERVED IN OTHER EXPERIMENTS

Some structures have been observed at other masses. The deuteron break-up experiment [37] analysis, concluded to the existence of structures for the following masses:

$M_X \approx 2.02 \pm 0.01$ GeV ($\Gamma_{1/2} \approx 0.045 \pm 0.02$ GeV) for Mnp invariant mass, $M_X \approx 2.03 \pm 0.02$ GeV ($\Gamma_{1/2} \approx 0.075 \pm 0.02$ GeV) for M_{NN} invariant mass and $M_X \approx 2.39 \pm 0.02$ GeV ($\Gamma_{1/2} \approx 0.06 \pm 0.02$ GeV) for $M_{NN\pi^+}$ invariant mass. We should notice that the first analysis of deuteron break-up experiment from Tokyo [40], more recent but with even poorer statistical yield, was not in good agreement with the data presented by the Warsaw group [37]. A new analysis of the Tokyo experiment [46] reveals some structures, but with a statistical significance still too small to reach any conclusion. The ^{4}He break up experiment analysis [38] with [dppn] final state, reported the existence of a structure in the invariant mass of two protons at 2.035 ± 0.015 GeV ($\Gamma_{1/2} \approx 0.030 \pm 0.023$ GeV), identified with 3.0 standard deviations. The ^{4}He break-up experiment analysis [38] with [ppppπ^-n] final state reported a peak for a pp invariant mass of 2.036 ± 0.15 GeV ($\Gamma_{1/2} \approx 0.027 \pm 0.025$ GeV). A pion production experiment ($pp \rightarrow d\pi^+$) [42] from LNS reported a narrow structure for $T_p = .35$ GeV which

corresponds to an invariant mass of 2.044 GeV. There is also a narrow structure at 2.014 GeV reported [43] from Bonn in two protons invariant mass studied by mean of $\gamma d \rightarrow pp\pi^-$ experiment. The two proton invariant mass observed using incident 5 GeV/c pions on ^{12}C (propane bubble-chamber) at Dubna, revealed a peak for a mass (FWHM) of 2.024 ± .003 GeV (.021 ± .015 GeV) [44].

4.8. GENERAL DISCUSSION

All data, those collected during the experiments $^3He(p,d)X$ and $p(^3He,d)X$ and those recalled in the previous section have been plotted in figure 20. It is obvious that they concentrate around some masses and are not randomly distributed, giving strong evidence for the existence of narrow B = 2 states.

Are these states created by strong NΔ coupling ? One such state has been predicted theoretically [55] in the analysis of π-nucleus scattering, but no theory can explain the existence of many of them. One argument favors such an hypothesis : a search for isoscalar dibaryons [56] has not been able to find them with a limit, on $d\sigma/dt$, of a few tenths of pb/GeV^2. This is two orders of magnitude lower than the excitation cross sections found in the B = 2, T = 1 search described in this paper. The experiment was a missing mass measurement from d+d → d+X reaction. However, since incident and target deuterons are loosely bound structures, their large radii can lead to a strong reduction of the production cross sections [41]. Then, in spite of the fact that we have not been able to observe isoscalar dibaryon resonances in an experiment especially designed to see them, we will not consider the NΔ explanation for the dibaryons observed here. The main reason is that we think it is difficult to understand how the large width $\Gamma_{1/2} \simeq .115$ GeV of the Δ resonance can be so reduced when bound with only one nucleon. The coupling of Δ with nuclei generally leads to a smaller reduction of the width remaining as large as 55-60 MeV [57].

The dibaryon at 2.124 GeV has a mass lower than $M_N + M_\Delta$ (2.17 GeV). It will most probably desexcite into NNπ. Since the N-π interaction in s state is rather "weak", the relatively small width of this state can be qualitatively understood. An explanation relating the dibaryons observed to interferences between different partial wave amplitudes has been proposed. For example Hollas [58], using the Mandelstam prediction [59] that singlet NN partial waves produce pions at a lower momenta than do triplet partial waves, concluded that

no resonant behavior was required to describe the structures observed in $\Delta\sigma_T$ and $\Delta\sigma_L$. However such an explanation disagrees with the observed features in our experiment of several narrow peaks stable in mass for different kinematical conditions and not symmetric with regard to $M_X + M_\Delta = 2.17$ GeV. A narrow quasi-bound state was predicted some years ago by Arenhövel [60], as formed by (NΔ) system. Since it was at a mass lower than 2.17 GeV (2.13 - 2.16 GeV) and with isospin T = 2, (forbidding decay into the NN channel) such an explanation is not satisfactory in our case. It is obvious that more theoretical effort has to be done within such a model to be more conclusive.

Another way to explain the existence of the observed narrow dibaryons is to describe them as states of six quarks coupled in a configuration other than $q^3 - q^3$. Many theoretical works have been done in this framework, usually within the MIT-type bag model [1]. Many states are then predicted. Few authors have tackled the problem of the calculation of their widths : Dorkin et al. [63], using a coupled channel method between 6 quarks and NN channels, have found for a simplified assumption of a single state of six quarks in S wave, a width close to 20 MeV for NN scattering at $T_p = .3$ GeV. Matveev [64] predicted the contribution of a single gluon exchange process to a hidden color state to the width to be close to 10 MeV. We notice that the calculated values of widths are close to the experimental ones presented in this work. Grein et al. [28] have calculated the dibaryons relative decay into π^+d and π^+np. We believe that a theoretical understanding of the widths of the states discussed here may have fundamental implications connected to the confinement of quarks.

Although calculated from the color magnetic gluon interaction [39] and not from a rotating fluxtube a mass formula of a rotational like type was predicted : $M = M_o + M_\perp J(J + 1)$. Figure 21 shows that the results fit nicely such mass formula. This allows the spin attribution which is given in table 2. The state at $M_X \approx 2.155$ was observed though not so clearly. With the state at $M_X \approx 2.192$ GeV, this defines a second rotational like band which appears as being less firm. However there is one property which is in favour of the existence of that second rotationnaly like band :

- the slope parameter found, $M_\perp = 18.7$ MeV, is the same for the two bands. We note that the two band heads have masses close to $2M_N + M_\pi$ and $2(M_N + M_\pi)$ respectively.

The ratio of the experimental values of M_0 and M_1 to the theoretical quantities found by Mulders [39] is close to 0.95. He used a bag radius of 1.31 fm. Using the same parameter values we get, for I = 1, J = 0,1,2,3, quantum numbers, radii varying from 1.31 to 1.36 fm. If we choose a mean value for the bag radius of 1.35 fm, we get M_1 = 19 MeV -very close to the experiment- instead of 19.7 MeV found by Mulders. But then the corresponding M_0 value equals 2.246 GeV instead of 2.126 GeV (Mulders) or 2.014 GeV (experiment).

Using the experimental mass formula, predictions for masses for isospin I = 0, 1 and 2 and spins J = 0, 1, 2, 3 and 4 are given in table 2. All the I = 1 states corresponding to the first rotational like band have been experimentally observed. Only the two first states with I = 1 corresponding to the second rotational like band have been experimentally observed. The I = 0 and I = 2 states have not been observed.

Recent theoretical investigations, including pionic corrections to a six quark bag calculation [61], predict masses and quantum numbers different from those found experimentally. A prediction based on 6 quarks shell model in a jj coupling combined with a diquark cluster model [62] found 2.13 and 2.24 GeV for the position of the two first levels in very good agreement with some levels found in our work. Since in this theoretical work there is a partial degeneracy in spin and total degeneracy in isospin, too few levels have been found. The NN partial width predicted in the last theoretical work quoted is small, but there is no prediction for total widths.

5. CONCLUSION

We have measured missing mass spectra from ^{3}He(p,d)X and p(^{3}He,d)X reactions leading to T_X = 1 and B_X = 2 final states. The quasi-free scattering on the deuteron substructure of ^{3}He is clearly observed at all angles and energies. The good statistics and missing mass resolution for this inelastic channel with large momentum transfer, allows the observation of narrow states. These narrow states were observed although they stand on top of a relatively large background formed by non-resonant NΔ and NNπ final states. Individual peaks are not present for all kinematical conditions (angle and energy). The relative excitation

of the peaks and background, in addition to the experimental precision, allow the observation of these narrow structures only for some t values, (see fig. 19). The non-observation of these structures in some experiments (and some angles in $^3He(p,d)X$ measurements) is then related to kinematically unfavorable conditions.

We have shown that our results, together with others from different experiments, fit a rotational-like mass formula. Such a mass formula is predicted in the framework of a six quark MIT-like bag model. The states observed are either in a quark configuration different from q^3-q^3, or in a q^3-q^3 extraneous state (quantum numbers forbidding NN decay without quark rearangement). This can be considered as being an experimental signature of quark effects at intermediate energies.

ACKNOWLEDGMENTS

We wish to thank T. Bauer, F. Samaran and N. Willis for help in the writing of the computer code analysis. We wish to thank F. Sai, J. Saudinos and W. J. Schwille for communicating their data to us prior to publication. We thank C. Wilkin for stimulating discussions and help in writing this paper.

REFERENCES

[1] R.L. JAFFE and F.E. LOW, Phys. Rev. D19 (1979) 2105
A.Th.M. AERTS et al., Phys. Rev. D17 (1978) 260
P.J.G. MULDERS et al., Phys. Rev. D21 (1980) 2653
P.J.G. MULDERS et al. Phys. Rev. Lett. 24 (1978) 1543
C.W. WONG and K.F. LIU, Phys. Rev. Lett 41 (1978) 82
K.F. LIU and C.W. WONG, Phys. Lett. 113B (1982) 1
C.W. WONG et al., Phys. Rev. C22 (1980) 2523
S.M. DORKIN et al., Preprint Dubna P4-81-791 (in russian).

[2] A. YOKOSAWA, Phys. Reports 64 (1980) 47
I.P. AUER, et al., Phys. Lett. 70B (1977) 475
I.P. AUER, et al., Phys. Rev. Lett. 41 (1978) 354
Y. MAKDISI, et al., Phys. Rev. Lett. 45 (1980) 1529
I.P. AUER, et al., Phys. Rev. D24 (1981) 2008
I.P. AUER, et al., Phys. Rev. Lett. 46 (1981) 1177
I.P. AUER, et al., Phys. Rev. Lett. 48 (1982) 1150
G.R. BURLESON, et al., Nucl. Phys. B213 (1983) 365
W.R. DITZLER, et al., Phys. Rev. D27 (1983) 680
I.P. AUER, et al., Phys. Rev. D29 (1984) 2435.

[3] I.P. AUER, et al., Phys. Rev. D29 (1984) 2435
T.S. BHATIA, et al., Phys. Rev. Lett. 49 (1982) 1135

[4] E. APRILE-GIBONI et al., Phys. Rev. D27 (1983) 2600 ; Phys. Rev. Lett. 46 (1981) 1047

[5] J. BYSTRICKY et al., Phys. Lett. 142 (1984) 130

[6] V.A. ANDREW, et al., Yad. Fiz. 35 (1982) 1457
A.V. DOBROVOLSKY, et al., Nucl. Phys. B214 (1983) 1

[7] D. AXEN, et al., J. Phys. G : Nucl. Phys. 7 (1981) L225
A.S. CLOUGH, et al., Phys. Rev. C21 (1980) 988
J.P. STANLEY, et al., Nucl. Phys. A403 (1983) 525

[8] J. BYSTRICKY, et al., Nuovo cimento 1984, DPh PE 82-12, DPh PE 82-09
K. HASHIMOTO, et al., Prog. of Theo. Phys., 64 (1980) 1678
H. HIDAKA, et al., Physics Letters 70B (1977) 479
K. HASHIMOTO and N. HOSHIZAKI, Prog. of Theo. Phys. 64 (1980) 1693
D.V. BUGG, et al., Phys. Rev. C21 (1980) 1004

[9] I.P. AUER, et al., Phys. Rev. Lett. 51 (1983) 1411
A.D. HANCOCK, et al., Phys. Rev. C27 (1983) 2742
T. RUPP et al., Phys. Rev C28 (1983) 1696
T.S. BHATIA, et al., Phys. Rev. C28 (1983) 2071

[10] G. GLASS, et al., Phys. Lett. 123 (1983) 27

[11] W.M. KLOET and R.R. SILBAR, Nucl. Phys. A364 (1981) 346
J.H. GRUBEN and B.J. VERWEST, Phys. Rev. C28 (1983) 836
B.J. VERWEST and R.A. ARNDT, Phys. Rev. C25 (1982) 1979
W. GREIN and P. KROLL, Nucl. Phys. A377 (1982) 505
W. GREIN, et al., Phys. Lett. 96B (1980) 176
W.M. KLOET, et al., Phys. Lett. 99B (1981) 80
W.M. KLOET and J.A. TJON, Phys. Lett. 106B (1981) 24
F. SHIMIZU, et al., Nucl. Phys. A389 (1982) 445
T. UEDA, Phys. Lett. 141B (1984) 157
W.M. KLOET and R.R. SILBAR, Phys. Rev. Lett. 45 (1980) 970
V.S. BHASKIN and I.M. DUCK, Nucl. Phys. B64 (1973) 269
B. BLANKLEIDER and I.R.AFNAN, Phys. Rev. C24 (1981) 1572
B.J. EDWARDS and G.H. THOMAS, Phys. Rev. D22 (1980) 2772
T. UEDA Phys. Lett. 74B (1978) 123 ; Phys. Lett. 119B (1982) 28.
M. ARAKI et al., Nucl. Phys. A389 (1982) 605
J.A. NISKANEN, Phys. Lett. 112B (1982) 17
W.M. KLOET and J.A. TJON, Nucl. Phys. A392 (1983) 271
J.A. TJON and E. VAN FAASSEN, Phys. Lett. 120B (1983) 39
W.M. KLOET and J.A. TJON, Phys. Rev. C27 (1983) 430
S.Y. TSAI, Progress of Theor. Phys. 64 (1980) 1710
L.A. KONDRATYUK and I.S. SHAPIRO, Sov. Jour. Nucl. Phys. 12 (1971) 220
R. BHANDARI et al., Phys. Rev. Lett. 46 (1981) 1111
M. ROSINA and M.J. PIRNER, Nucl. Phys. A367 (1981) 398
H. SATO and K. SAITO, Phys. Rev. Lett. 50 (1983) 648
M. CVETIC-KRIVEE et al., Phys. Lett. 99B (1981) 486

[12] B.J. EDWARDS, Phys. Rev. D23 (1981) 1978

[13] W. JAUCH, A. KONIG and P. KROLL, Phys. Lett. 143B (1984) 509
L.G. DAKHNO, et al., Phys. Lett. 114B (1982) 409

[14] B.G. RITCHIE, et al., Phys. Rev. C24 (1981) 552
B. MAYER et al., Nucl. Phys. A437 (1985) 630

[15] H. GARCILAZO, Phys. Rev. Lett. 45 (1980) 780
J.A. NISKANEN, Phys. Lett. 141B (1984) 301
D.V. BUGG, J. Phys. G : Nucl. Phys. 10 (1984) 717, 10 (1984) 47
J. DUBACH, et al., Phys. Lett. 106B (1981) 29
M.M. MAKAROV, et al., Phys. Lett. 122B (1983) 343
A.V. KRAVTSOV, et al, J. Phys. G : Nucl. Phys. 9 (1984) L187
T. MIZUTANI, et al., Phys. Lett. 107B (1981) 177

[16] M.G. DOSH, et al., Phys. Rev. C29 (1984) 1549
H. GARCILAZO, Phys. Rev. Lett. 48 (1982) 577
E. FERREIRA and G.A. PEREZ MUNGUIA, J. Phys. G : Nucl. Phys. 9 (1983) 169
A.S. RINAT and J. ARVIEUX, Phys. Lett. 104B (1981) 182
A. MATSUYAMA and K. YAZAKI, Nucl. Phys. A364 (1981) 477
W. GREIN and M.P. LOCHER, J. Phys.G : Nucl. Phys. 7 (1981) 1355
K. KUBODERA et al., J. Phys. G : Nucl. Phys. 6 (1980) 171
J. ARVIEUX and A.S. RINAT, Nucl. Phys. A350 (1980) 205
K. KUBODERA and M.P. LOCHER, Phys. Lett. 87B (1979) 169

[17] M. AKEMOTO et al., Phys. Rev. Lett. 51 (1983) 1838 ; Phys. Rev. Lett. 50 (1983) 400
J.H. HOFTIEZER, et al., Phys. Rev. C23 (1981) 407 ; Phys. Lett. 100B (1981) 462

[18] J. BOLGER et al., Phys. Rev. Lett. 48 (1982) 1667, Phys. Rev. Lett. 46 (1981) 167

[19] E.L. MATHIE et al., Phys. Rev. C28 (1983) 2558
G.R. SMITH et al., Phys. Rev. C29 (1984) 2206

[20] H. GARCILAZO, Phys. Rev. Lett. 53 (1984) 652
A.S. RINAT, Phys. Lett. 126B (1983) 151

[21] J. ULBRICHT et al., Phys. Rev. Lett. 48 (1982) 311
W. GRUEBLER et al., Phys. Rev. Lett. 49 (1982) 444
V. KONIG et al., J. Phys. G : Nucl. Phys. 9 (1983) L211

[22] E. UNGRICHT et al., Phys. Rev. Lett. 52 (1984) 333
E. UNGRICHT et al., Phys. Rev. C31 (1985) 934

[23] G.G. SMITH, et al., Phys. Rev. C30 (1984) 980

[24] G. GLASS et al., Phys. Rev. Lett. 53 (1984) 1[illegible]

[25] T. KAMAE et al., Phys. Rev. Lett. 38 (1977) 468
T. KAMAE and T. FUJITA, Phys. Rev. Lett. 38 (1977) 471
H. IKEDA, et al., Phys. Rev. Lett. 42 (1979) 1321, Nucl. Phys. B172 (1980) 509

[26] P.E. ARGAN et al., Phys. Rev. Lett. 46 (1981) 96

[27] K. BABA, et al., Phys. Rev. Lett. 48 (1982) 729 ; Phys. Rev. C28 (1983) 286
T. ISHII et al., Phys. Lett. 110B (1982) 441

[28] W. GREIN, K. KUBODERA and M.P. LOCHER, Nucl. Phys. A356 (1981) 269

[29] R.R. SILBAR, Comments Nucl. Part. Phys. 12 (1984) 177
A. SVARC, Invited Talk at the PANIC 84, Conference Heidelberg
E.L. LOMON, Invited Talk at the High Energy Spin Phys. Conference, Marseille 1984
P. KROLL, Unpublished WU.B.83-8
K.K. SETH, Proc. of High Energy Photo Nucl. React and Relat., Topics, Tokyo 1983 ; and to be published.

[30] M.H. MACGREGOR, Phys. Rev. Lett. 42 (1979) 1724
T.H. FIELDS and A. YOKOSAWA, Phys. Rev. D21 (1980) 1432

[31] J. WAINER and E. LOMON Phys. Rev. D22 (1980) 1217

[32] P.J.G. MULDERS, Phys. Rev. D25 (1982) 1269 ; Phys. Rev. D26 (1982) 3039 ; Phys. Rev. D28 (1983) 443

[33] P.W. LISOWSKI et al., Phys. Rev. Lett. 49 (1982) 255
R.E. SHAMU et al., Phys. Rev. D25 (1982) 2008

[34] M. GARCON et al., Rapport DPhN/Saclay, n°2234, 1985 ; to be published ; see also ref. [54].

[35] K.K. SETH et al., Proceedings from Karlsruhe Conference 1983, p. 93.

[36] B. TATISCHEFF, et al., Phys. Rev. Lett. 52 (1984) 2022
B. TATISCHEFF, et al., Proceedings of the X International Conf. on Part. and Nuclei, Heidelberg, 1984, Contributed paper C7.

[37] T. SIEMIARCZUK et al., Phys. Lett. 128B (1983) 367
T. SIEMIARCZUK et al., Phys. Lett. 137B (1984) 434
B.S. ALADASHVILI et al., Nucl. Phys. A274 (1976) 486

[38] V.V. GLAGOLEV et al., Zeitschrift für Physik 317 (1984) 335
P. ZELINSKI et al., Proceedings of JINR, Dubna 1-83-565, 1-83-566 (in russian).

[39] P.J.G. MULDERS, A.Th.M. AERTS and J.J. DE SWART, Phys. Rev. Lett. 40 (1978) 1543.

[40] N. KATAYAMA, et al., Nucl. Phys. A423 (1984) 410

[41] C. WILKIN, Private Communication

[42] J. SAUDINOS et al., Proceedings of "Nucl. Phys. in GeV region", meeting KEK, Nat. Lab., Japan, 1984.

[43] W.J. SCHWILLE, Private communication, and B. BOCK et al., Contribution to the 11th Europhysics Conference Nuclear Physics with Electromagnetic Probes, Paris 1985.

[44] A.A. BAIRAMOV et al., Sov. J. Nucl. Phys. 39 (1984) 26

[45] S. BUHLER, Proc. 8th Int. Cryogenic Engineering Conf. Berlin, May 1980.

[46] F. SAI, Private Communication

[47] J. THIRION et al., Note CEA N-1248,
A. BOUDARD, Rapport interne, LNS, p. D1.

[48] H. QUECHON, Thèse de doctorat d'Université, Orsay (1980)

[49] J. SAUDINOS et al., N.I.M. III (1973) 77

[50] T. BAUER, et al., unpublished

[51] B. BRICAUD et al., IEEE Trans. Nucl. Sci. NS26 (1979) 4641

[52] F. JAMES, CERN library program W505.

[53] J. ZABOLITZKY and W. EY, Phys. Lett. 76B (1978) 527

[54] M. GARCON, Thesis, 1985, unpublished.

[55] M.G. HUBER, H.G. HOPF and M. DILLIG, Proceedings of the IUCF Workshop, Bloomington, 1984

[56] M.P. COMBES-COMETS, et al., Nucl. Phys. A431 (1984) 703

[57] C.L. MORRIS, et al., Phys. Lett. 123B (1983) 37
C. ELLEGAARD, et al., Phys. Rev. Lett. 50 (1983) 1745
B. TATISCHEFF, et al., Phys. Lett. 77B (1978) 254

[58] C.L. HOLLAS, Phys. Rev. Lett. 44 (1980) 1166

[59] S. MANDESLTAM, Proc. Phys. Soc. A244 (1958) 491

[60] H. ARENHOVEL, Nucl. Phys. A247 (1975) 473

[61] P.J.G. MULDERS and A.W. THOMAS, J. Phys. G : Nucl. Phys. 9 (1983) 1159

[62] N. KONNO, et al., Lettere al Nuovo Cimento 34 (1982) 313
N. KONNO, Private Communication.

[63] S.M. DORKIN et al., Dubna preprint, E2-80-43

[64] V.A. MATVEEV, Dubna preprint D1,2 - 12036, 1978, p. 137 (in russian)

[65] D. LEGRAND Thèse d'Etat, Université Paris VI 1979
R. FRASCARIA et al., Nucl. Phys. A264 (1976) 445

TABLE 1

Number of standard deviations (S.D.) from the background of the narrow structure and corresponding confidence levels (C.L.). The masses (M_X), total widths at half maximum ($\Gamma_{1/2}$) and cross sections ($d\sigma/dt$) correspond to the structures found.

TABLE 2

Masses of I = 0,1 and 2, J = 0,1,2,3 and 4 dibaryons deduced from the measured levels using the band head at 2.014 GeV (first rotational band), and the band head at 2.155 GeV (second rotational band).

	Angle	S.D.	C.L.	M_x (GeV)	$\Gamma_{1/2}$ (GeV)	$d\sigma/dt(\mu b/GeV^2)$	$-t\ (GeV^2)$
	M_x = 2.24 GeV						
p(^{3}He,d)X	17°64	3.10	99.8 %	2.245 ± .002	.016 ± .003	7.3 ± 2.0	
$T_{^3He}$ = 2.7 GeV	18°	1.40	83.8 %	2.237 ± .002	.015 ± .004	2.8 ± 1.1	- .04
	18°36	0.74	54.1 %	2.232 ± .003	.018 ± .007	2.5 ± 1.4	
^{3}He(p,d)X							
T_p = .925 GeV (N 80)	40°	2.73	99.4 %	2.243 ± .003	.017 ± .006	1.3 ± .57	.96
.925 (N 79)	40°	5.64	(> 99.9 %)	2.241 ± .002	.024 ± .004	2.32 ± .50	.96
	M_x = 2.12 GeV						
.925	40°	6.94	(> 99.9 %)	2.121 ± .001	.025 ± .002	1.46 ± .15	.89
.750	40°	2.89	99.6 %	2.128 ± .005	.024 ± .011	.864 ± .53	.59
	M_x = 2.19 GeV						
.750	40°	4.13	(> 99.9 %)	2.192 ± .003	.025 ± .006	4.16 ± 1.34	.63

TABLE 1

	First Rotational Band			Second Rotational Band		
	I = 0	I = 1	I = 2	I = 0	I = 1	I = 2
J = 0	1.902	2.0147	2.239	2.042	2.155	2.379
J = 1	1.940	2.052	2.276	2.080	2.192	2.416
J = 2	2.012	2.124	2.348	2.152	2.264	2.488
J = 3	2.128	2.240	2.464	2.268	2.380	2.604
J = 4	2.276	2.388	2.612	2.416	2.528	2.752

TABLE 2

FIGURE CAPTIONS

Fig. 1 – Beam line

Fig. 2 – Lay-out of the detection system (not to scale). A,B,C,D,F are scintillation counters hodoscopes. Ω is the (virtual) source point for trajectories entering the spectrometer along its optical axis.

Fig. 3 – Typical time of flight spectra

Fig. 4 – Bi-dimensional spectrum e versus M_x

Fig. 5 – Shows the overlap of different runs to get the missing mass spectra for $2.085 < M_x < 2.28$ GeV, and the effect of a correction factor $(1/\sigma)(d\sigma/d\Theta) = 3.6\ 10^{-3}$/ mrad : ϕ (without correction : x).

Fig. 6 – $^3He(p,p)^3He$ elastic scattering cross sections

Fig. 7 – Comparison of some results obtained with different computers, computer codes, and cuts.

Fig. 8 – Comparison of some results obtained at different dates

Fig. 9 – Missing mass spectrum for $T_p = .925$ GeV and $\Theta_d = 40°$ lab. The full curves correspond to polynomial and polynomial plus Gaussian fits. The dashed curve is the normalized phase space ($X = N\Delta$, $\Gamma_{1/2} = .115$ GeV for the Δ). Data have been binned into 5 MeV intervals.

Fig. 10 – Same caption as in figure 9 but for $T_p = .75$ GeV

Fig. 11 – Corresponding empty target spectrum. The arrows show the full minus empty target cross section (see fig. 10).

Fig. 12 – Same caption as in figure 9 for dashed curve but for $T_p = .925$ GeV, $\Theta_d = 30°$ lab. The full line is drawn by hand.

Fig. 13 – Same caption as in figure 12 but for $T_p = .75$ GeV, $\Theta_d = 32°$ lab.

Fig. 14 – Same caption as in figure 12 but for $T_p = .75$ GeV, $\Theta_d = 22°$ lab.

Fig. 15 – Kinematics for $p(^3He,d)X$ reaction

Fig. 16 – Missing mass spectra for $p(^3He,d)X$ reaction at $T_p = 2.7$ GeV and $\Theta_d = 17°64$, 18° and 18°36. The full lines correspond to polynomial and polynomial + gaussian fits.

Fig. 17 – Normalised phase space calculations for $p(^3He,d)X$ reaction. The dashed curve (dot-dashed) corresponds to $X = N\Delta$ ($\Gamma_{1/2} = .115$ GeV) ($X = NN$). The full curves correspond to polynomial fit and a curve drawn by hand to get the broad bump excitation cross section.

Fig. 18 – Missing mass spectra for $^3He(p,d)X$ reaction at $T_p = .925$ and .750 MeV, $\Theta_d = 40°$ lab. showing the presence of the states at $M_x = 2.124$, 2.192 and 2.243 GeV.

Fig. 19 - Domain of missing mass (M_X) and transfer (t) covered in our measurements. The full circles give the position of observed structures, while the open ones refer to indications for a structure.

Fig. 20 - Display of the narrow dibaryon masses found in the different experiments.

Fig. 21 - Same as figure 20, but with an empirical assignment of spin, showing evidence for a rotational-like mass formula $M = M_o + M_\perp J(J + 1)$.

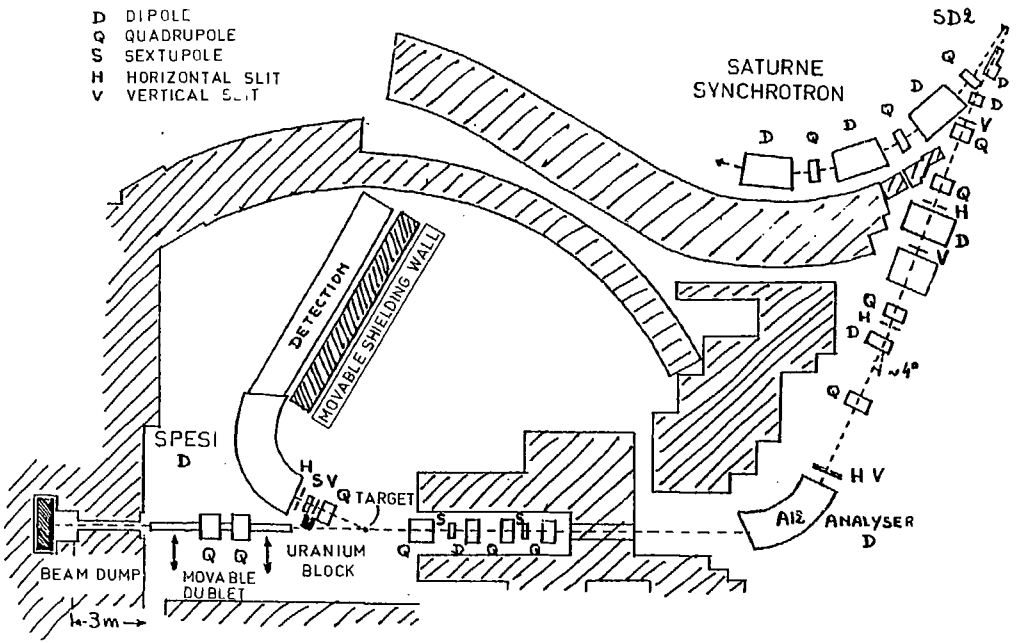
D DIPOLE
Q QUADRUPOLE
S SEXTUPOLE
H HORIZONTAL SLIT
V VERTICAL SLIT
SATURNE
SYNCHROTRON
SD2
DETECTION
MOVABLE SHIELDING WALL
SPESI
D
H
V
Q
TARGET
S
Q Q
MOVABLE
DUBLET
URANIUM
BLOCK
BEAM DUMP
~3m
~4°
H V
AI2
ANALYSER
D

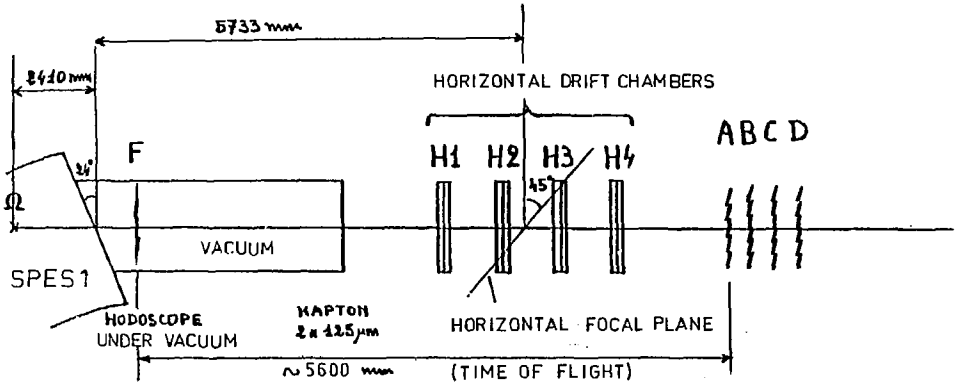
5733 mm
2410 mm
HORIZONTAL DRIFT CHAMBERS
ABCD
F
H1 H2 H3 H4
24°
45°
Ω
VACUUM
SPES1
HODOSCOPE
UNDER VACUUM
KAPTON
2 x 125 μm
HORIZONTAL FOCAL PLANE
~5600 mm
(TIME OF FLIGHT)

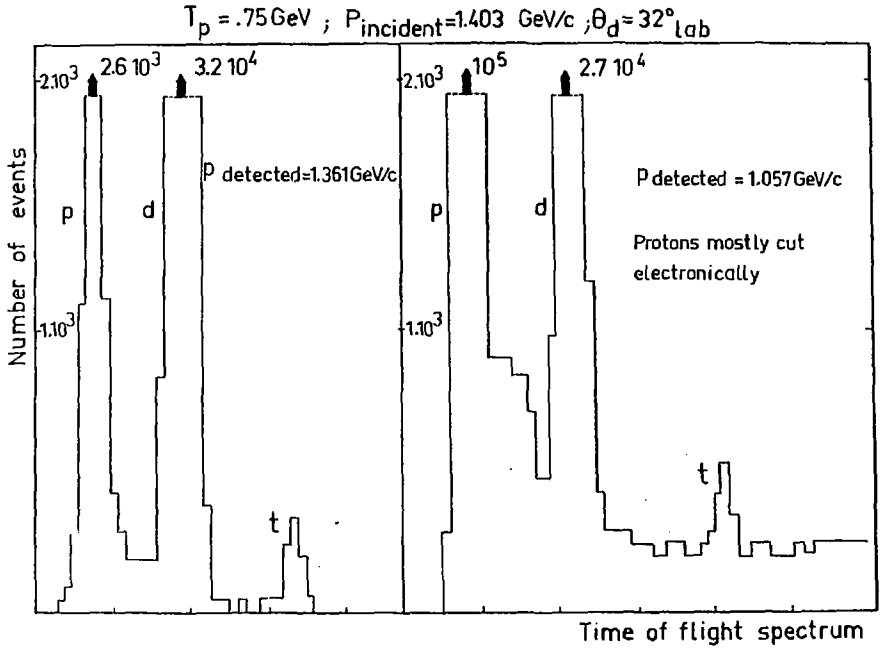
T_p = .75 GeV ; $P_{incident}$=1.403 GeV/c ; θ_d = 32° lab
2.10³
2.6 10³
3.2 10⁴
p
d
t
P detected=1.361GeV/c
1.10³
Number of events
2.10³
10⁵
2.7 10⁴
P detected = 1.057GeV/c
Protons mostly cut electronically
1.10³
Time of flight spectrum

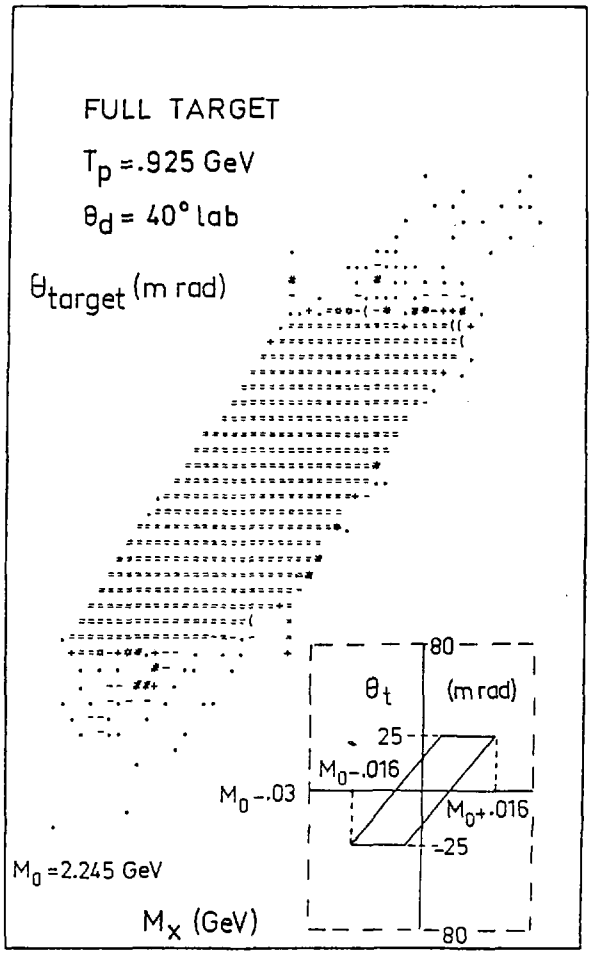
FULL TARGET
T_p = .925 GeV
θ_d = 40° lab
θ_{target} (m rad)
80
θ_t
(m rad)
25
M_0-.016
M_0 -.03
M_0+.016
-25
M_0 = 2.245 GeV
M_x (GeV)
80

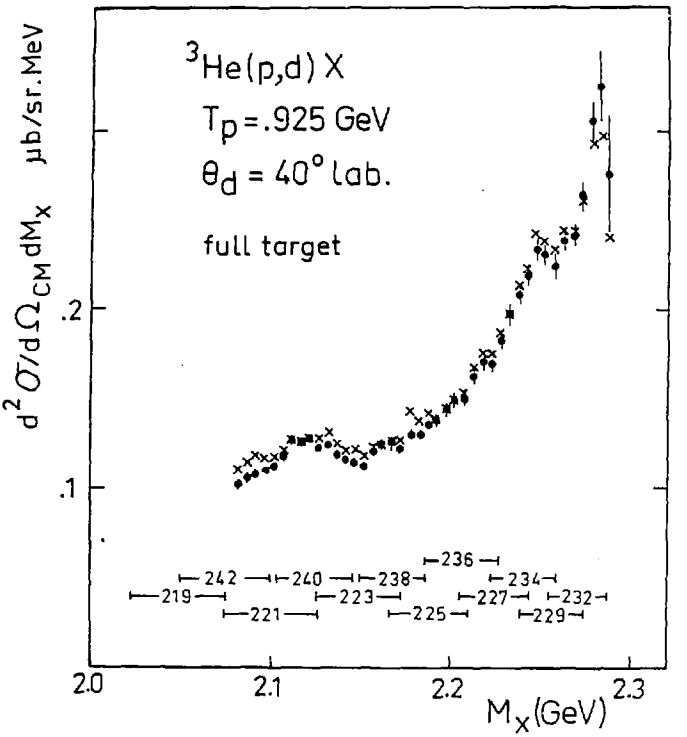
^{3}He(p,d) X
T_p = .925 GeV
θ_d = 40° lab.
full target
$d^2\sigma/d\Omega_{CM}dM_x$ μb/sr.MeV
.2
.1
2.0
2.1
2.2
2.3
M_x(GeV)
219
221
242
240
238
223
236
225
234
227
232
229

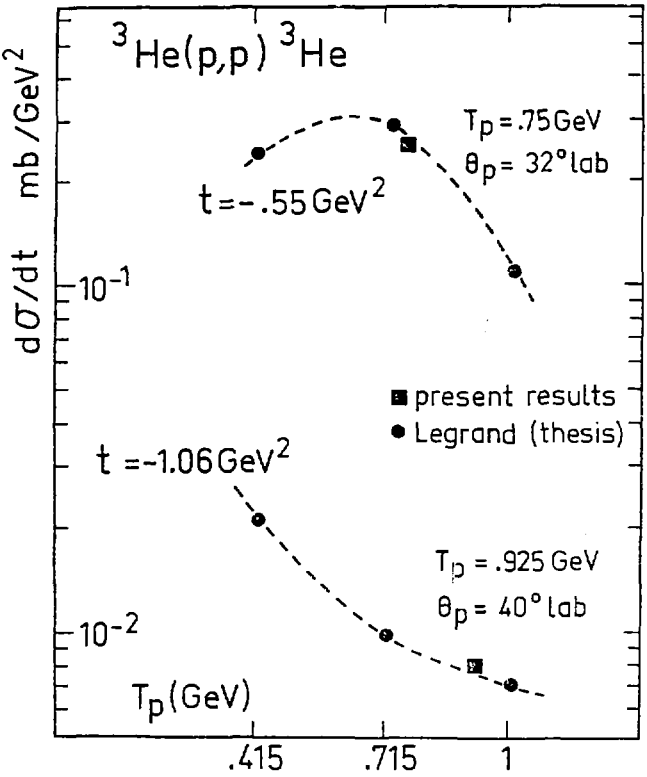
$^3He(p,p)\,^3He$
$d\sigma/dt$ mb/GeV^2
T_p = .75 GeV
θ_p = 32° lab
t = -.55 GeV^2
10^{-1}
present results
Legrand (thesis)
t = -1.06 GeV^2
T_p = .925 GeV
θ_p = 40° lab
10^{-2}
T_p(GeV)
.415
.715
1

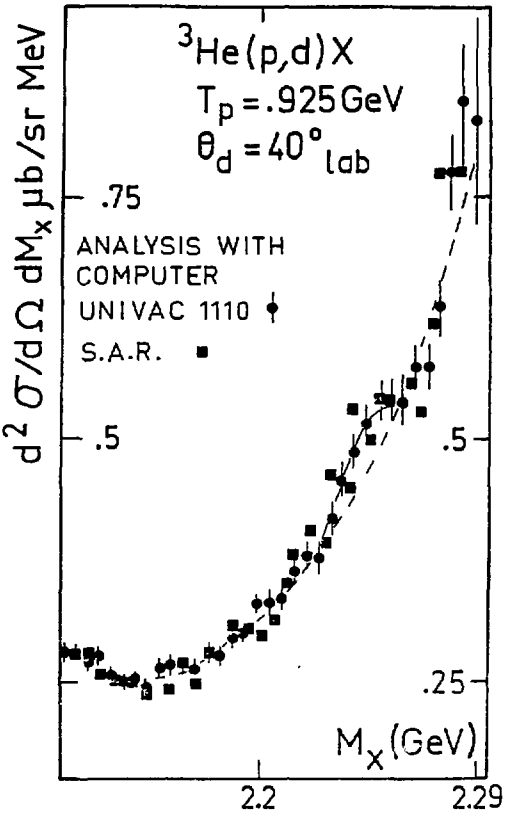
^{3}He(p,d)X
T_p = .925 GeV
θ_d = 40° lab
ANALYSIS WITH
COMPUTER
UNIVAC 1110
S.A.R.
$d^2\sigma/d\Omega\, dM_x$ μb/sr MeV
.75
.5
.5
.25
M_x (GeV)
2.2
2.29

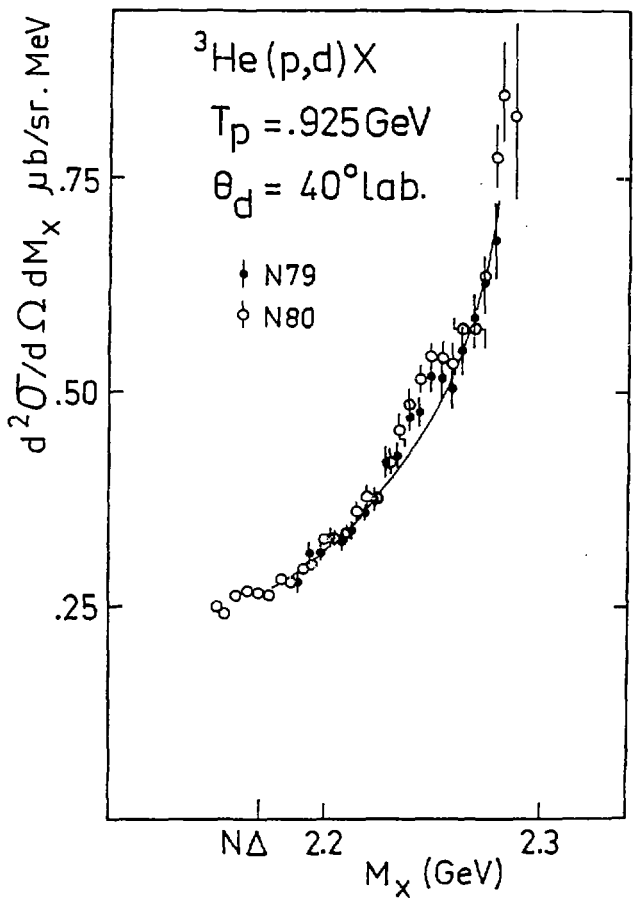
^{3}He (p,d) X
T_p = .925 GeV
θ_d = 40° lab.
N79
N80
$d^2\sigma/d\Omega\, dM_x$ μb/sr. MeV
.75
.50
.25
NΔ
2.2
2.3
M_x (GeV)

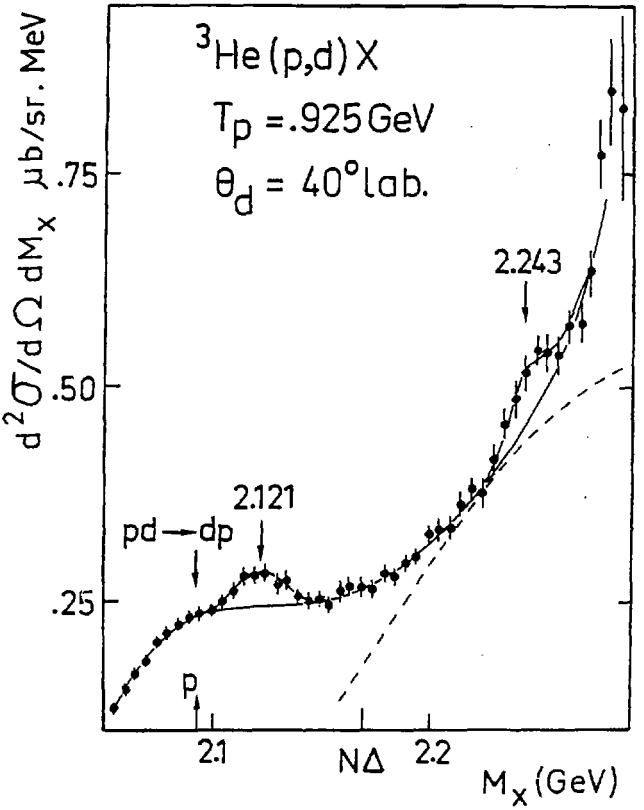
^{3}He(p,d)X
T_p = .925 GeV
θ_d = 40° lab.
$d^2\sigma/d\Omega\, dM_x$ μb/sr. MeV
.75
.50
.25
2.243
2.121
pd — dp
p
2.1
NΔ
2.2
M_x (GeV)

Fig. 9

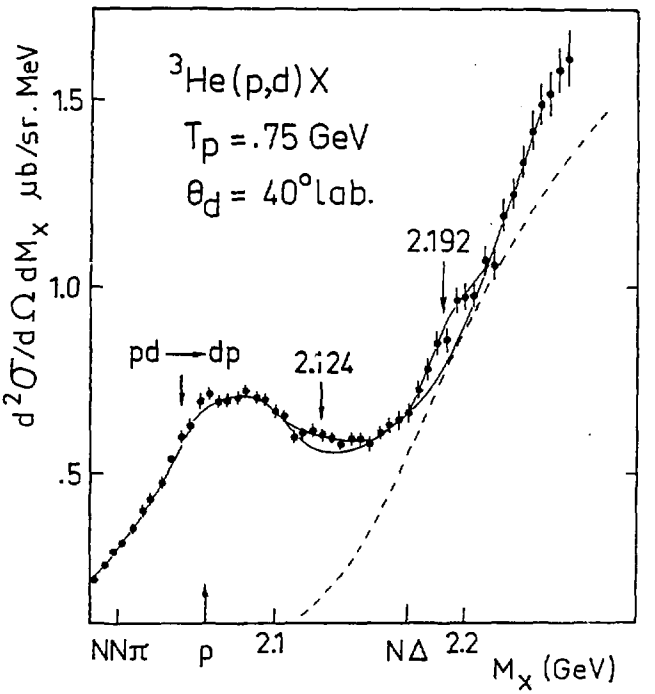
^{3}He(p,d)X
T_p = .75 GeV
θ_d = 40° lab.
$d^2\sigma/d\Omega\, dM_x$ μb/sr. MeV
1.5
1.0
.5
2.192
pd — dp
2.124
NNπ
p
2.1
NΔ
2.2
M_x (GeV)

Fig. 10

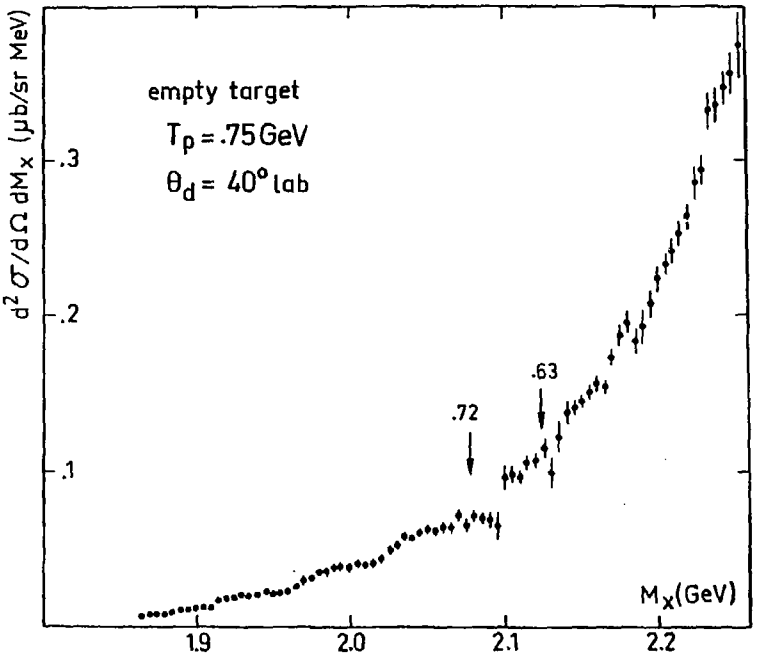
empty target
$T_p = .75\,GeV$
$\theta_d = 40°$ lab
$d^2\sigma/d\Omega\, dM_x$ (μb/sr MeV)
.3
.2
.1
.72
.63
M_x(GeV)
1.9
2.0
2.1
2.2

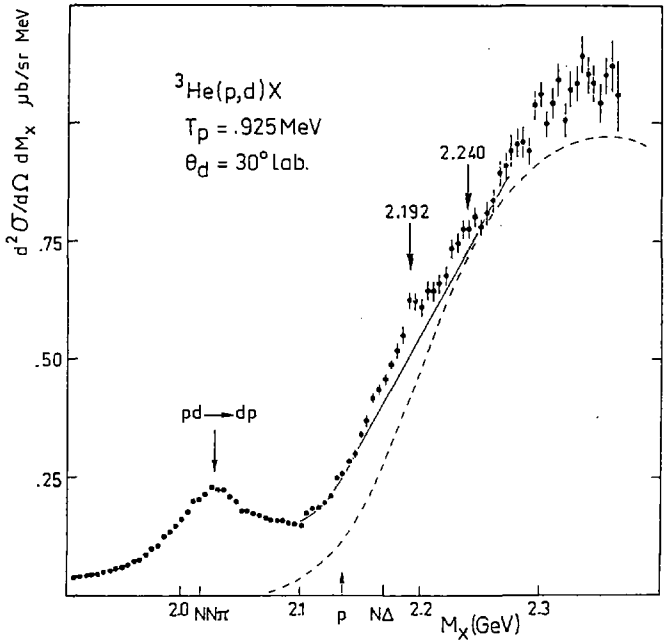
^{3}He(p,d)X
T_p = .925 MeV
θ_d = 30° lab.
2.240
2.192
pd → dp
$d^2\sigma/d\Omega\, dM_x$ μb/sr MeV
.75
.50
.25
2.0 NNπ
2.1
p
NΔ
2.2
2.3
M_X(GeV)

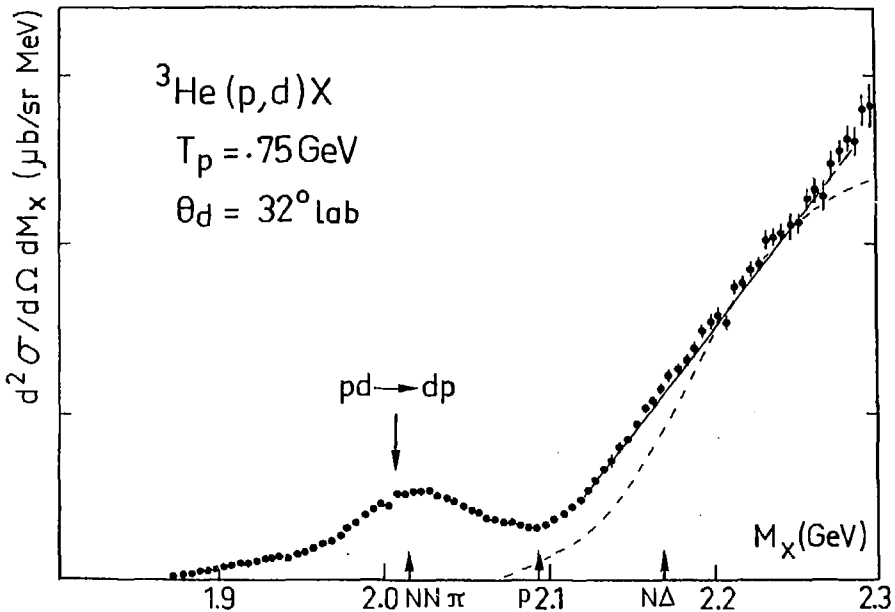
^{3}He (p,d) X
T_p = .75 GeV
θ_d = 32° lab
$d^2\sigma/d\Omega\, dM_X$ (μb/sr MeV)
pd → dp
M_X(GeV)
1.9
2.0 NN π
P 2.1
NΔ
2.2
2.3

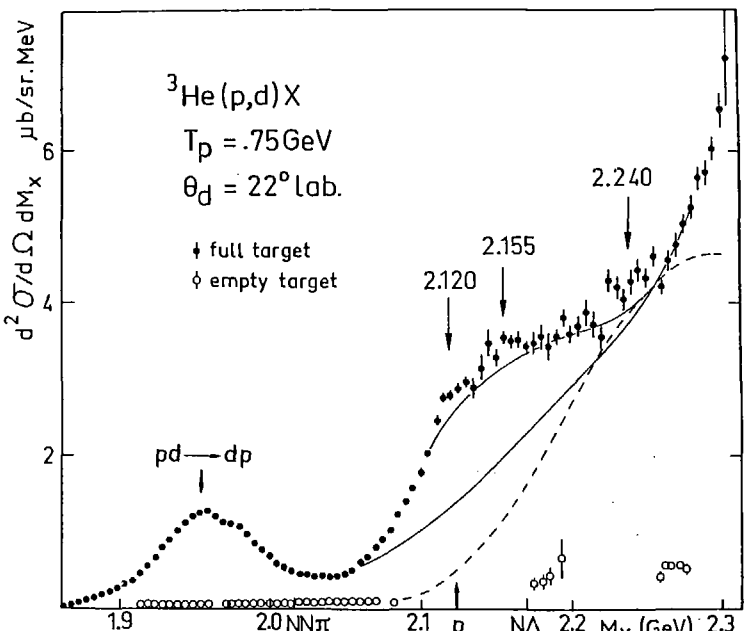
^{3}He (p,d) X
T_p = .75GeV
θ_d = 22° lab.
full target
empty target
2.120
2.155
2.240
pd → dp
$d^2\sigma/d\Omega\, dM_x$ μb/sr.MeV
6
4
2
1.9
2.0 NNπ
2.1
p
NΔ
2.2
M_x (GeV)
2.3

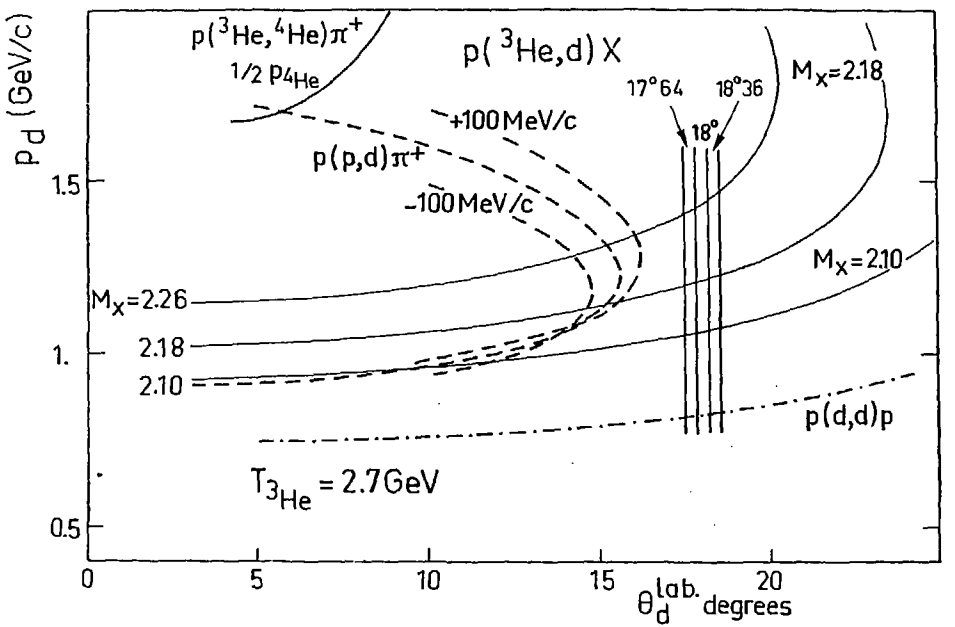
p(³He,⁴He)π⁺
1/2 p4He
p(³He,d) X
17°64
18°36
18°
Mx=2.18
+100MeV/c
p(p,d)π⁺
-100MeV/c
Mx=2.26
2.18
2.10
Mx=2.10
p(d,d)p
T3He = 2.7GeV
pd (GeV/c)
1.5
1.
0.5
0
5
10
15
20
θd lab. degrees

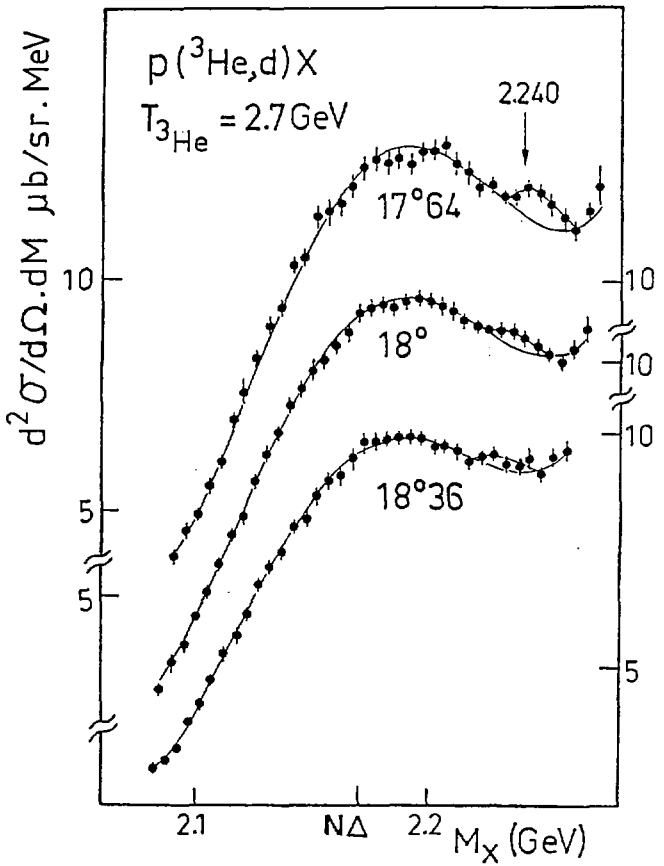
p(³He,d)X
T3He = 2.7 GeV
2.240
17°64
18°
18°36
d²σ/dΩ.dM μb/sr.MeV
10
5
5
10
10
10
5
2.1
NΔ
2.2
Mx (GeV)

Fig. 14

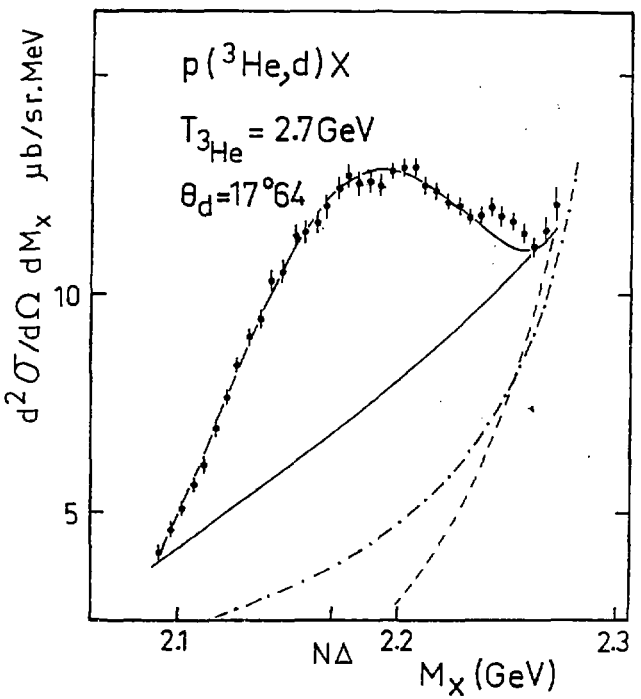
p(³He,d)X
T3He = 2.7GeV
θd=17°64
d²σ/dΩ dMx μb/sr.MeV
10
5
2.1
NΔ
2.2
2.3
Mx (GeV)

Fig. 17

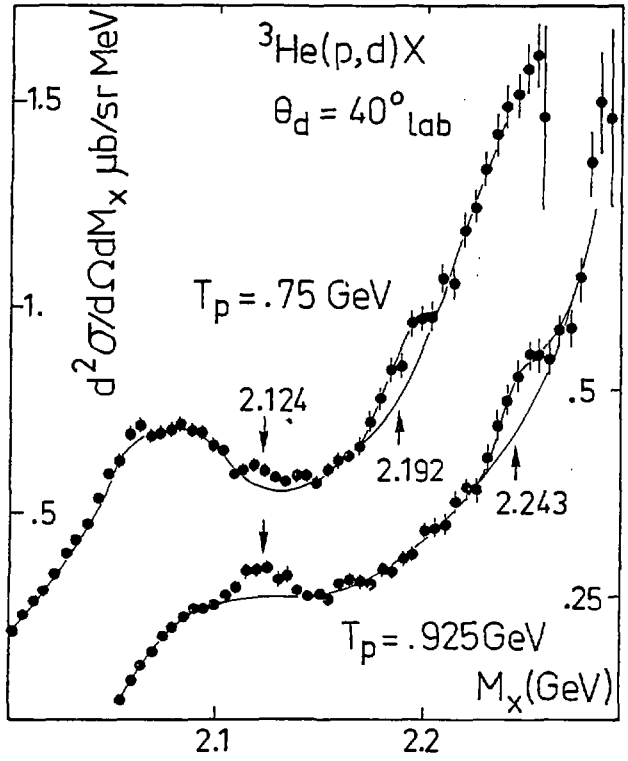
^{3}He(p,d)X
$\theta_d = 40°_{lab}$
$d^2\sigma/d\Omega dM_x$ μb/sr MeV
1.5
1.
.5
$T_p = .75$ GeV
2.124
2.192
2.243
.5
.25
$T_p = .925$GeV
M_x(GeV)
2.1
2.2

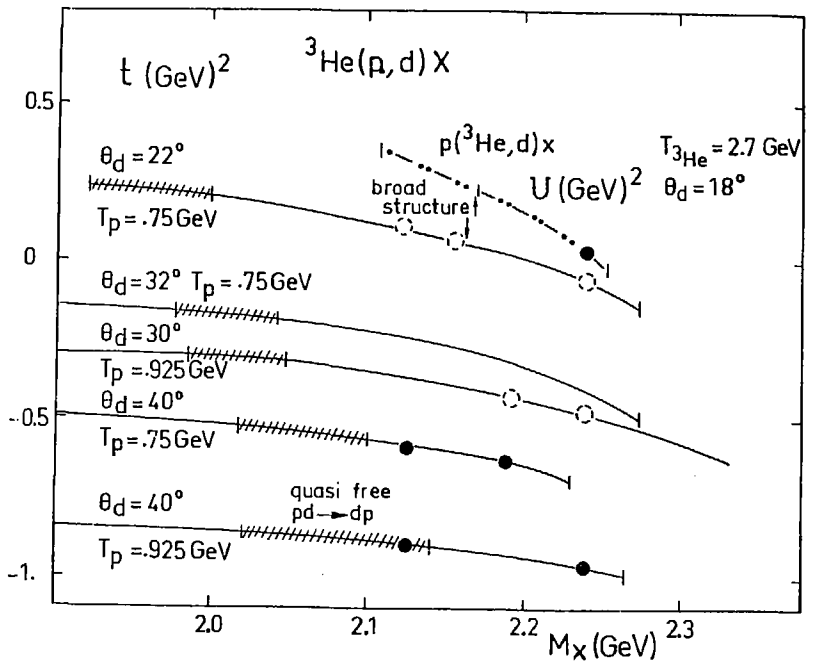
t (GeV)²
³He(p,d)X
0.5
0
-0.5
-1.
θd = 22°
Tp = .75 GeV
p(³He,d)x
broad structure
U (GeV)²
T3He = 2.7 GeV
θd = 18°
θd = 32° Tp = .75 GeV
θd = 30°
Tp = .925 GeV
θd = 40°
Tp = .75 GeV
θd = 40°
quasi free
pd → dp
Tp = .925 GeV
2.0
2.1
2.2
2.3
Mx (GeV)

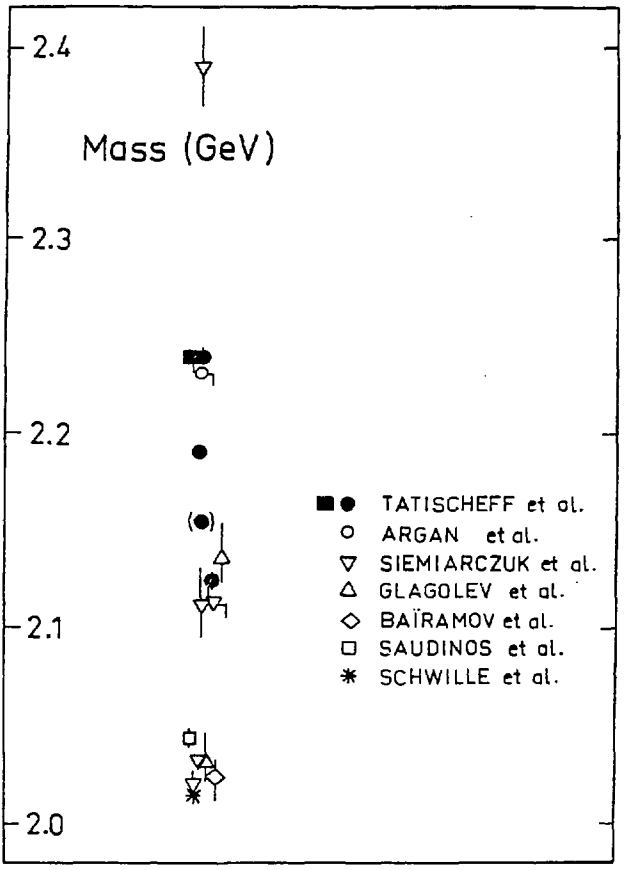
2.4
Mass (GeV)
2.3
2.2
2.1
2.0
TATISCHEFF et al.
ARGAN et al.
SIEMIARCZUK et al.
GLAGOLEV et al.
BAÏRAMOV et al.
SAUDINOS et al.
SCHWILLE et al.

Fig.20

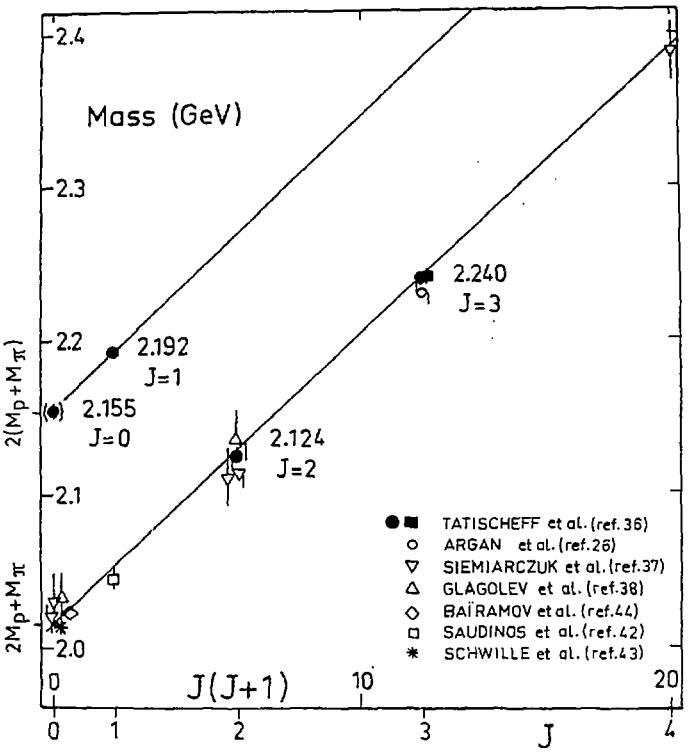
Mass (GeV)
2.4
2.3
2.2
2.1
2.0
2(Mp+Mπ)
2Mp+Mπ
2.240
J=3
2.192
J=1
2.155
J=0
2.124
J=2
TATISCHEFF et al. (ref. 36)
ARGAN et al. (ref. 26)
SIEMIARCZUK et al. (ref. 37)
GLAGOLEV et al. (ref. 38)
BAÏRAMOV et al. (ref. 44)
SAUDINOS et al. (ref. 42)
SCHWILLE et al. (ref. 43)
0
J(J+1)
10
20
0
1
2
3
J
4

Fig. 21